

Explicit simulation of gravity waves in a whole atmosphere model

Erich Becker

NorthWest Research Associates, Boulder, CO, USA

With contributions from:

S. Vadas, L. Harvey, L. Goncharenko, X. Chu, J. Huba, J. Oberheide

Some pros and cons of a conventional GCM with parameterized gravity waves (GWs)

PROS:

- computationally not very demanding, climatological runs
- major dynamical features of the general circulation of the lower and middle atmosphere are captured (including the cold summer mesopause and warm winter stratopause)
- self-induced simulation of the Quasi-Biennial Oscillation possible

...

Conventional GW schemes are based on strong assumptions (single column and steady state approximations) → CONS:

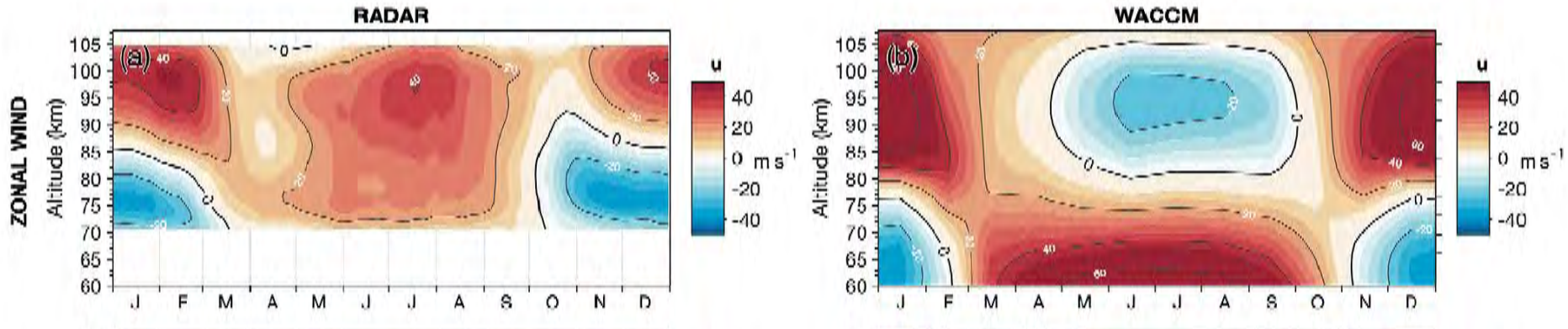
- launch level parameters instead of continuous sources
- spectrum of monochromatic waves instead of wave packets
- no lateral propagation
- no secondary or higher-order GWs, no GWs from the polar vortex

Consequences:

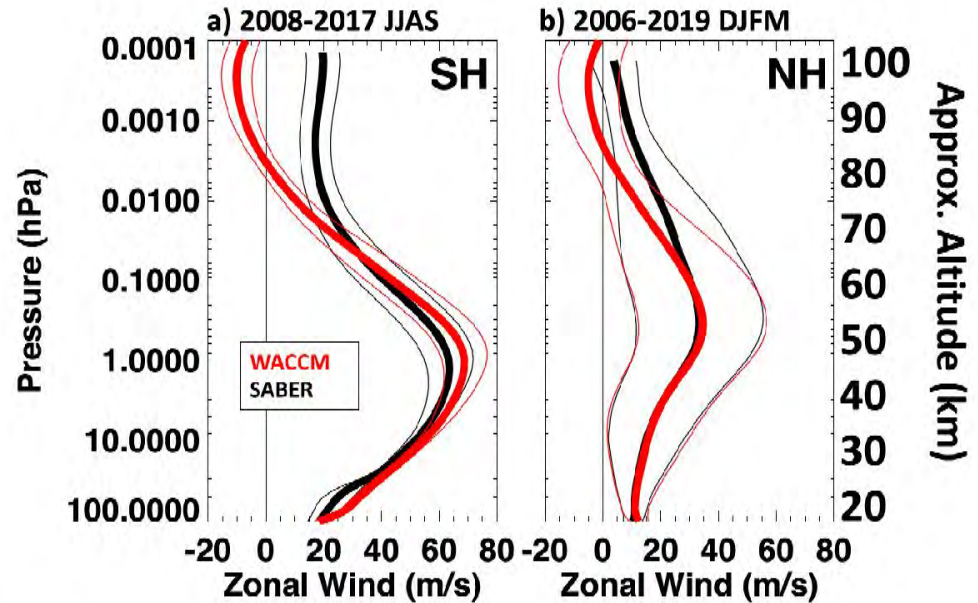
- wrong direction of the mean zonal flow in the winter mesopause region
- almost no GWs in the thermosphere (except for high-frequency GWs from deep convection)
- incomplete GW-tidal interaction

Fidelity of a GCM with parameterized GWs is better for weaker polar vortex

Mean zonal wind over South Georgia: Radar versus WACCM (from Hindley et al., 2022, ACP)

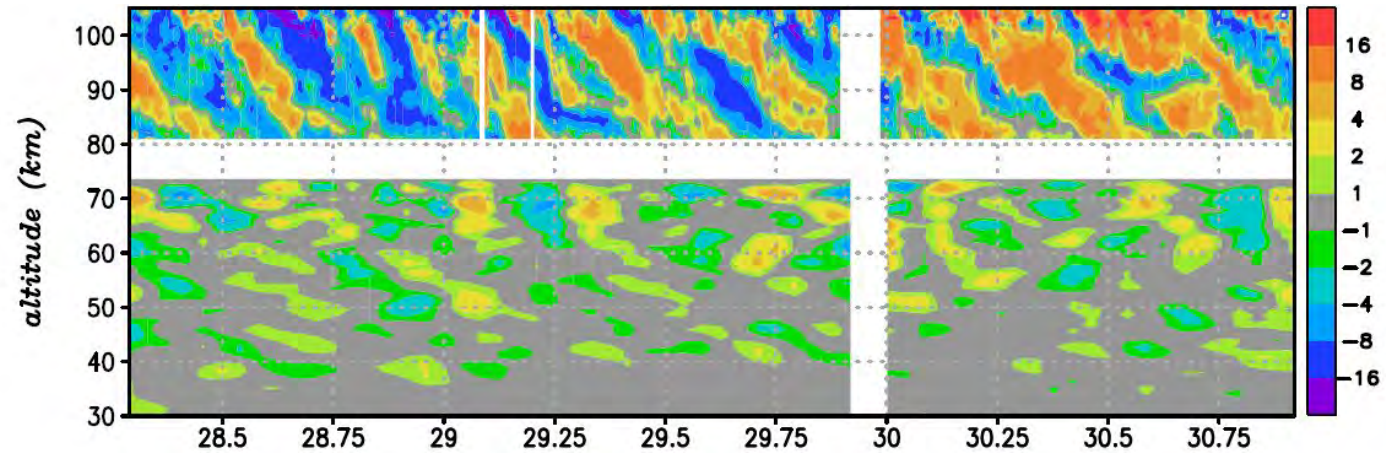


Wintertime zonal-mean zonal wind poleward of 40° : SABER versus WACCM (from Harvey et al., 2022, JGR-A)

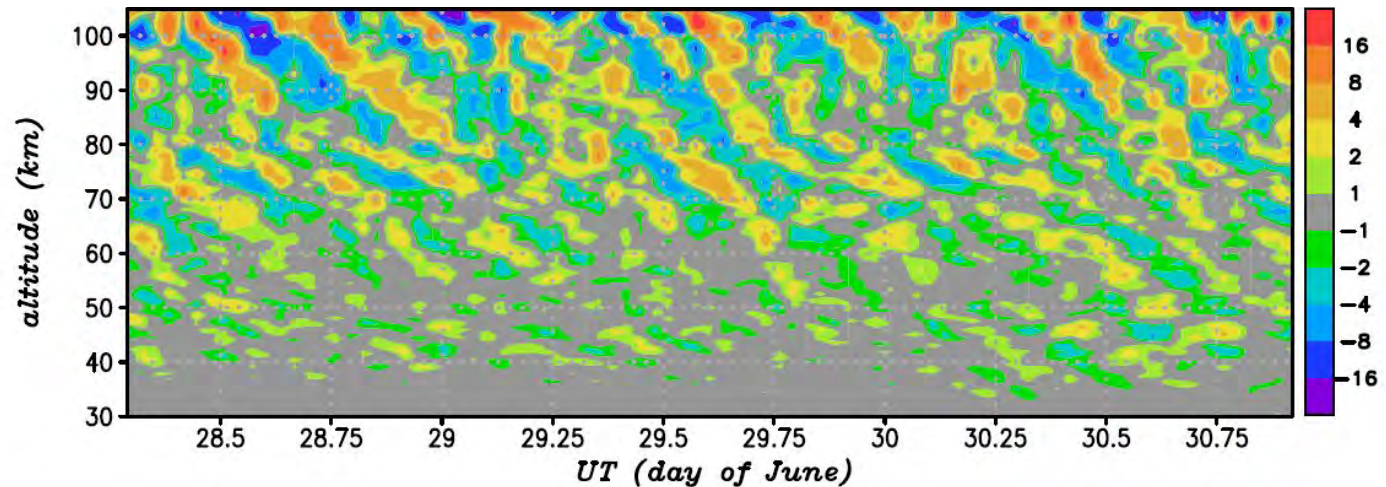


GWs in the winter mesopause region

Relative temperature variations over McMurdo (78S, 167E) during wintertime for periods < 12 h from lidar measurements (Chen, Chu et al., JGR-A, 2016)



Ditto from a GW-resolving general circulation model (Becker & Vadas, JGR-A, 2018)



Since the eastward mean zonal wind decreases with z in the winter mesosphere, the increase of λ_z with increasing z implies that the GWs in the mesopause region are eastward propagating.

HI Altitude Mechanistic general Circulation Model (HIAMCM)

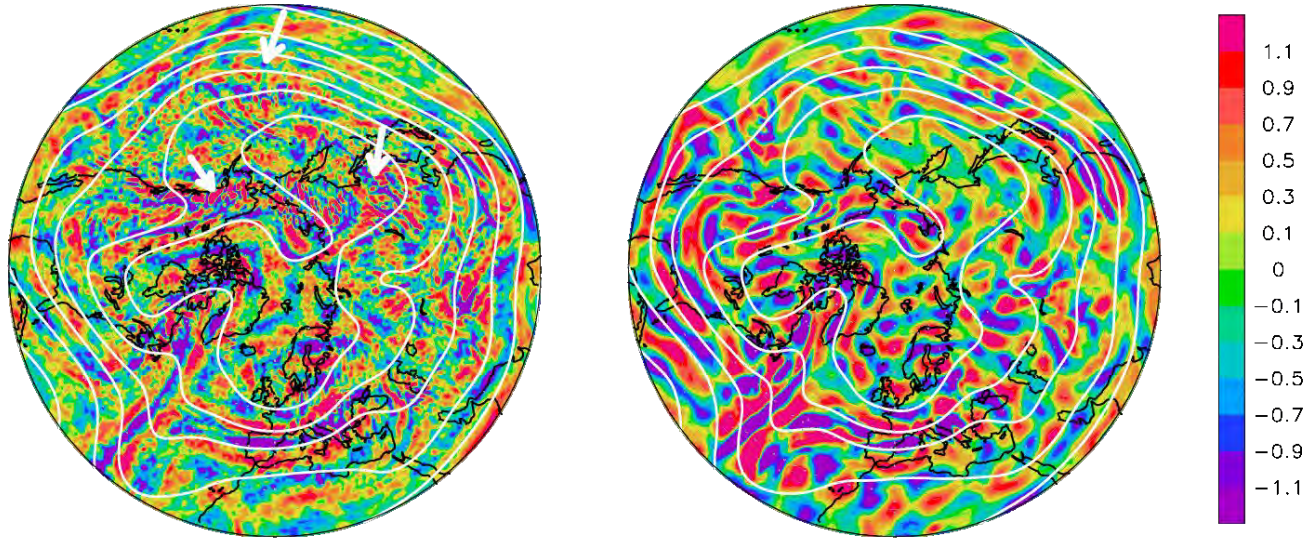
- spectral GCM with a terrain-following hybrid vertical coordinate; T256L280 up to 5×10^{-9} hPa (~ 450 km), $\Delta x \sim 52$ km, $\Delta z \sim 600$ m below ~ 130 km and coarser in the thermosphere (~ 5 km between 300 and 450 km)
- radiative transfer, tropospheric moisture cycle, full orography, slab ocean, thermodynamics with $R(p)$ and $c_p(T)$, correction for non-hydrostatic dynamics, ion drag (Becker & Vadas, JGR-SP, 2020)
- “mechanistic” because of 1) no chemistry, 2) simplified parameterizations for radiation and moist convection, 3) ion drag is the only ionospheric process
- nudging to MERRA-2 reanalysis in spectral space for the large scales only ($\lambda_h > 2000$ km) (Becker et al., JGR-A, 2022)

- non-resolved scales parameterized by **macro-turbulent vertical and horizontal diffusion** based on the classical Smagorinsky model extended by a Richardson number criterion (Becker, JAS, 2009)
- **molecular viscosity for both vertical and horizontal diffusion, no artificial sponge layer** (Becker & Vadas, JGR-SP, 2020)
- **gravity waves (GWs) simulated explicitly (generation, propagation, GW-mean flow interaction) by both the free-running and the nudged model, subject to the effective spatial resolution of $\lambda_h \sim 200$ km**

- **major assumption: unresolved GWs are local and represent a macro-turbulent inertial range**

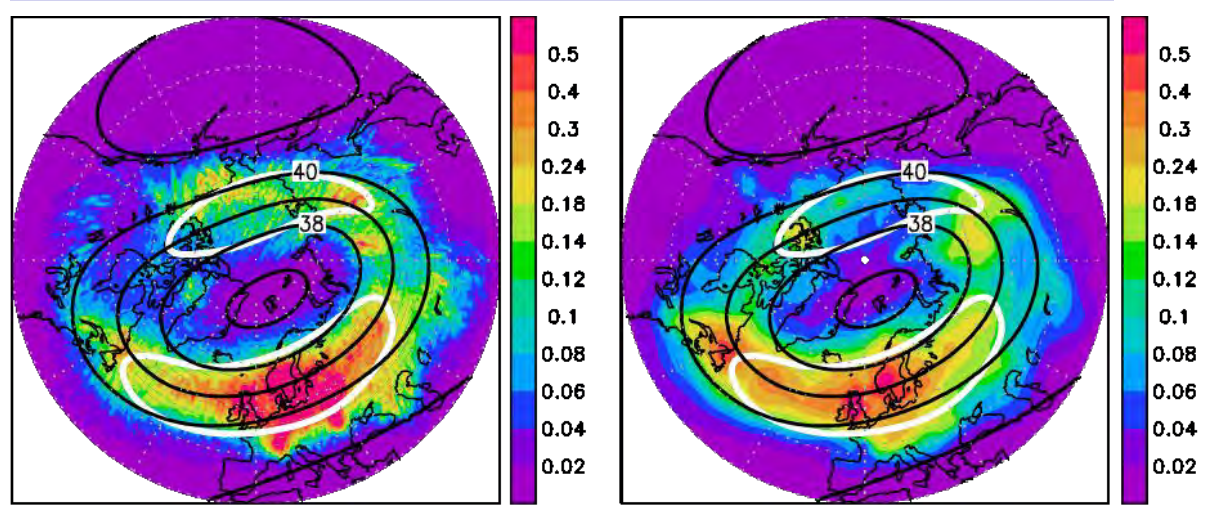
Resolved GWs:
Nudged
HIAMCM versus
MERRA-2,
12 Jan. 2016,
12UT

T' (K) and horiz. streamf. at 200 hPa
HIAMCM MERRA-2



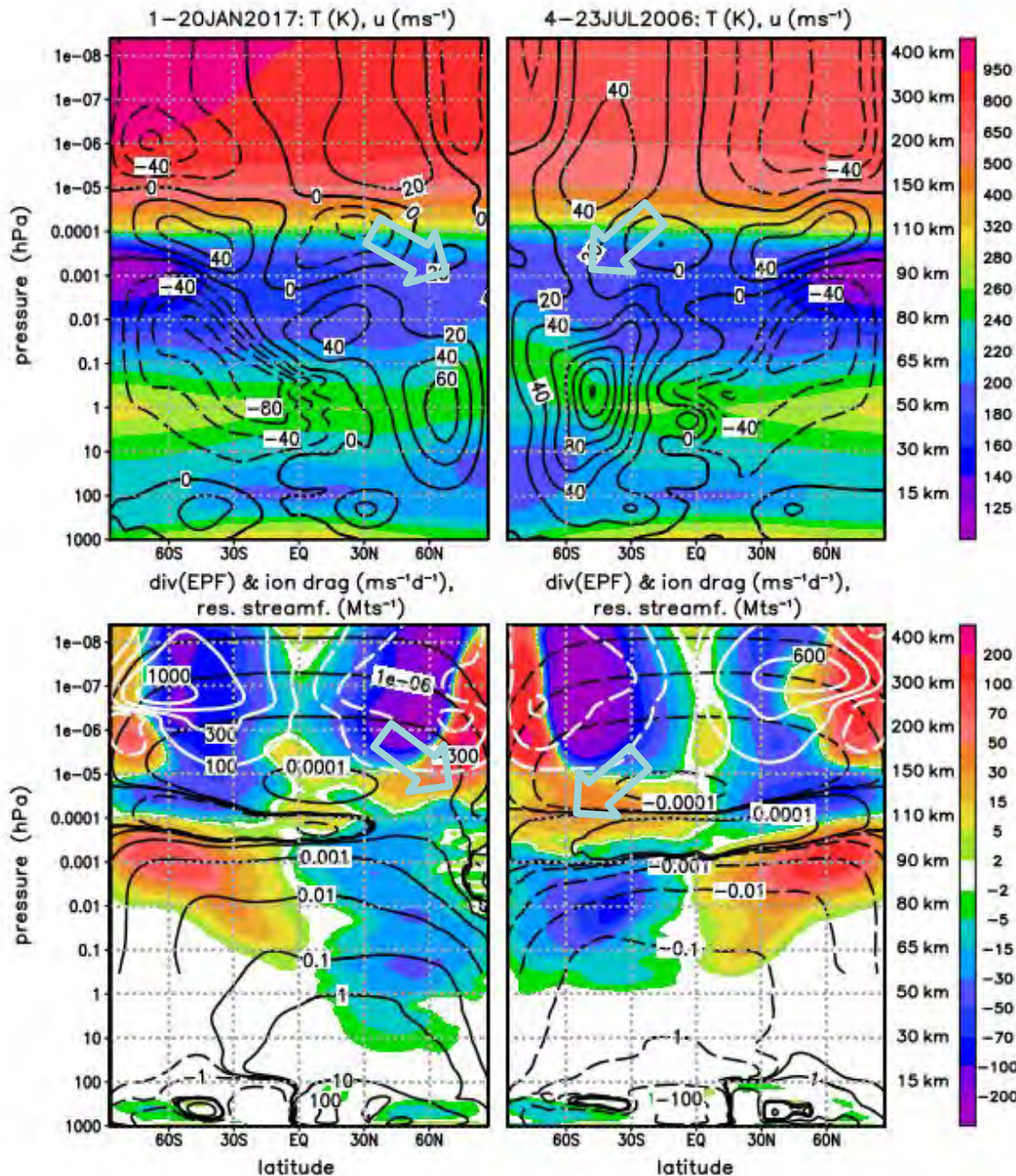
GWs in the
stratosphere:
Nudged
HIAMCM versus
AIRS,
1-31 Jan. 2016

T variance (K^2), z @ 2.4 hPa (km), $|v|$ (80 m/s)
HIAMCM AIRS



(Becker, Vadas, et al., 2022, JGR-A)

Zonal-mean circulation during January 2020 and July 2006



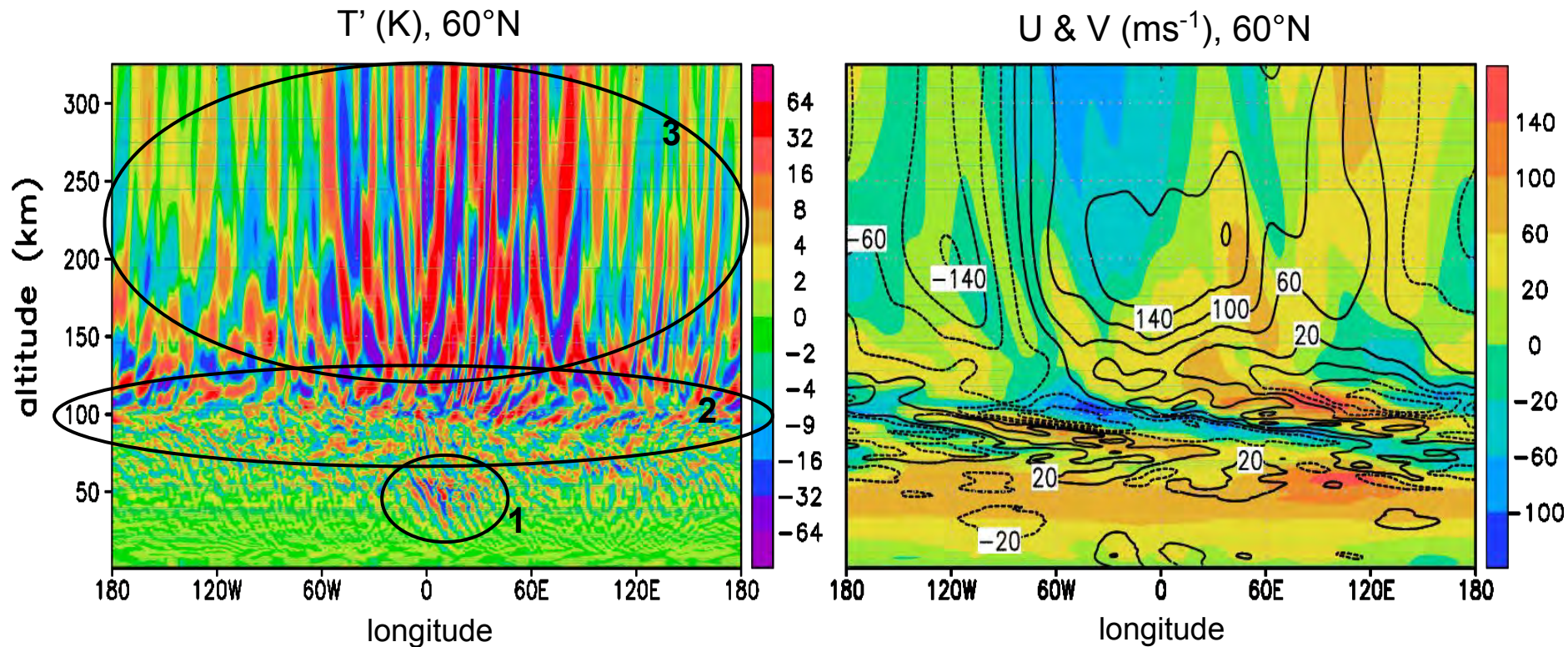
- Continuously eastward zonal wind in the winter mesopause region at high latitudes.

- Eastward EPF divergence in the winter mesopause region (due to mainly **se-condary GWs**, stronger in the SH because of the stronger polar vortex). → Reversed residual circulation extends to the winter pole during July

- Summer-winter circulation in the upper thermosphere driven by zonal ion drag. EPF divergence from waves (tides and GWs) is less important.

(Model data from Becker & Oberheide, GRL, 2023, *subm.*)

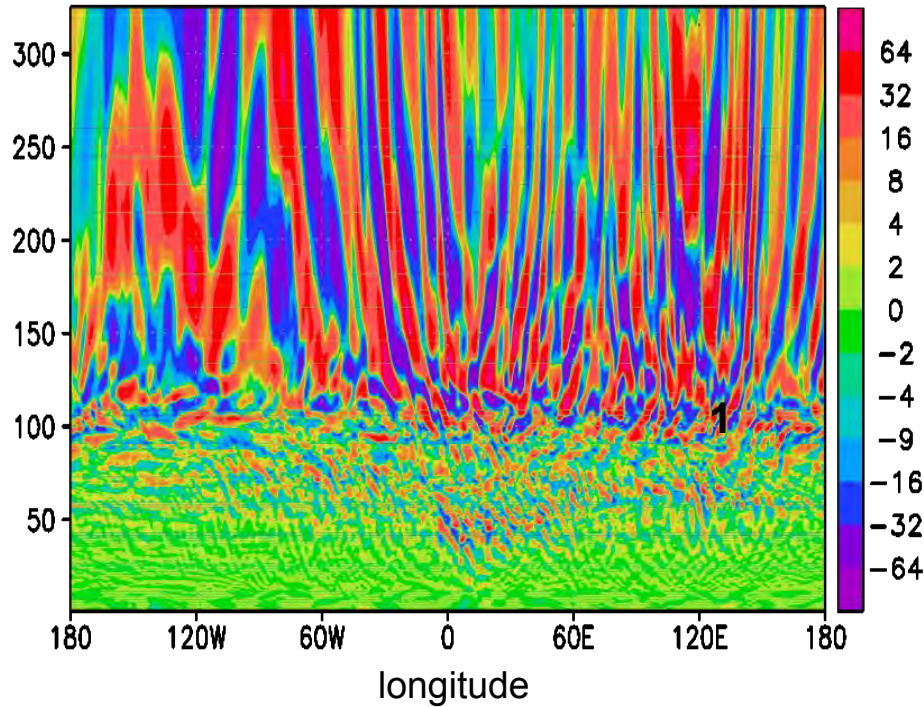
Multi-step vertical coupling during a strong polar vortex: 27DEC2016, 12:00 UT



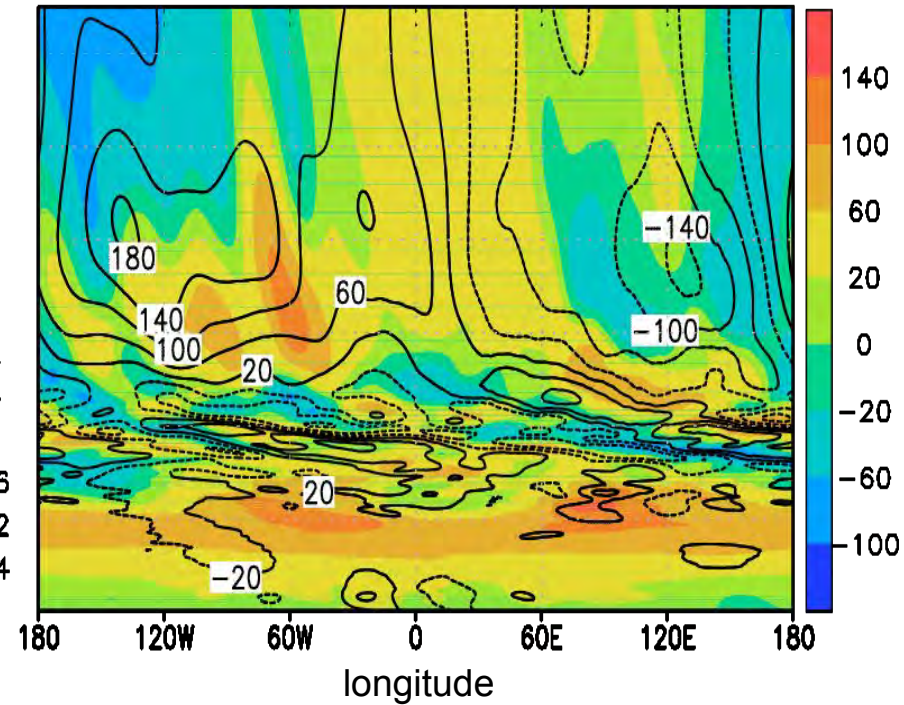
- (1)** Primary (westward) GWs (strongest over northern Europe), dissipating in the mesosphere due to $dU/dz < 0$.
- (2)** Secondary GWs (eastward and westward) in the mesosphere, dissipating in the lower thermosphere due to alternating large-scale tidal winds.
- (3)** Tertiary GWs in the thermosphere. Predominant propagation direction not clear from longitude-height plots.

Multi-step vertical coupling during a strong polar vortex: 27DEC2016, 19:30 UT

T' (K), 60°N



U & V (ms⁻¹), 60°N

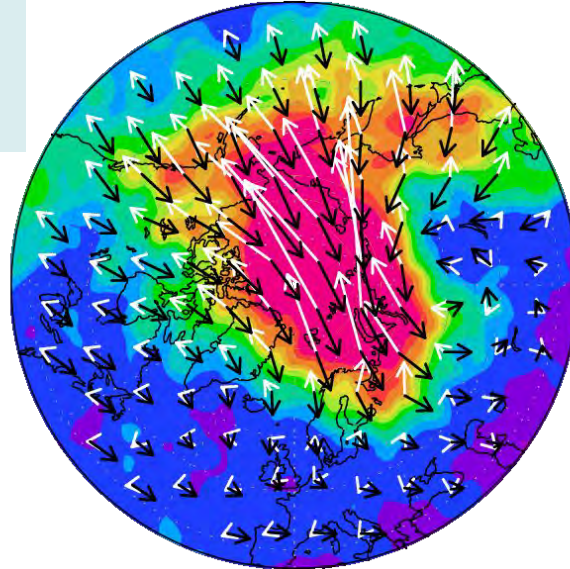


While the GWs in the stratosphere do not change very much during 7.5 hours, wind-induced directional dissipation/filtering due to westward propagating tides (and traveling PWs) become increasingly evident at higher altitudes.

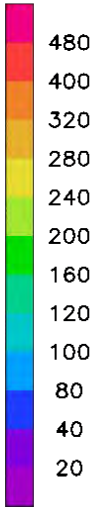
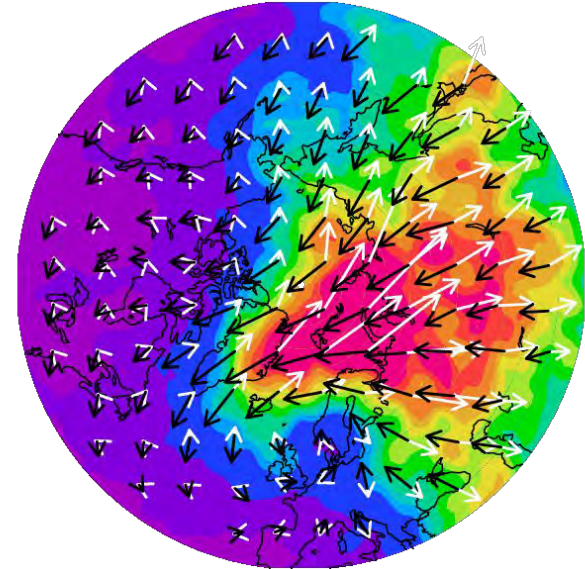
Averaged daily cycle in the thermosphere during the strong polar vortex period (21-30DEC2016)

21DEC–30DEC2016, 10^{-7} hPa (~ 300 km):
GW kin. energy (m^2s^{-2}) & (U,V) (ms^{-1}) & GW mom. flux (m^2s^{-2})

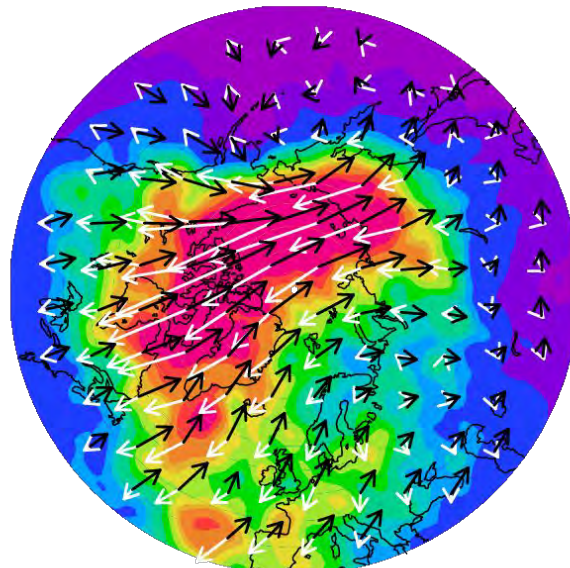
(a) 0 UT



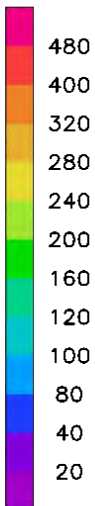
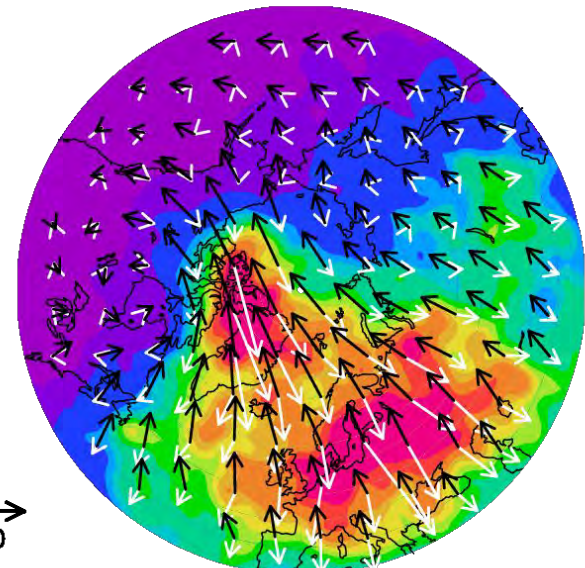
(b) 6 UT



(c) 18 UT



(d) 12 UT



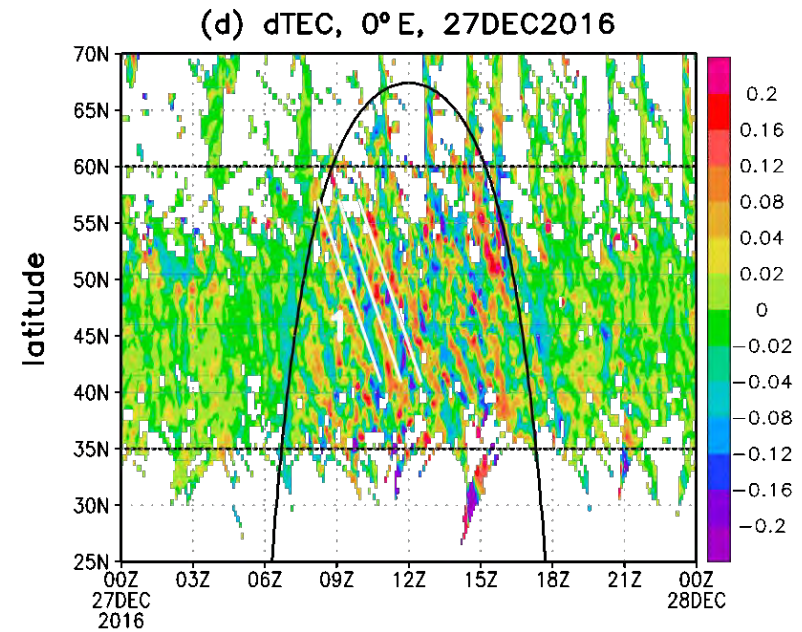
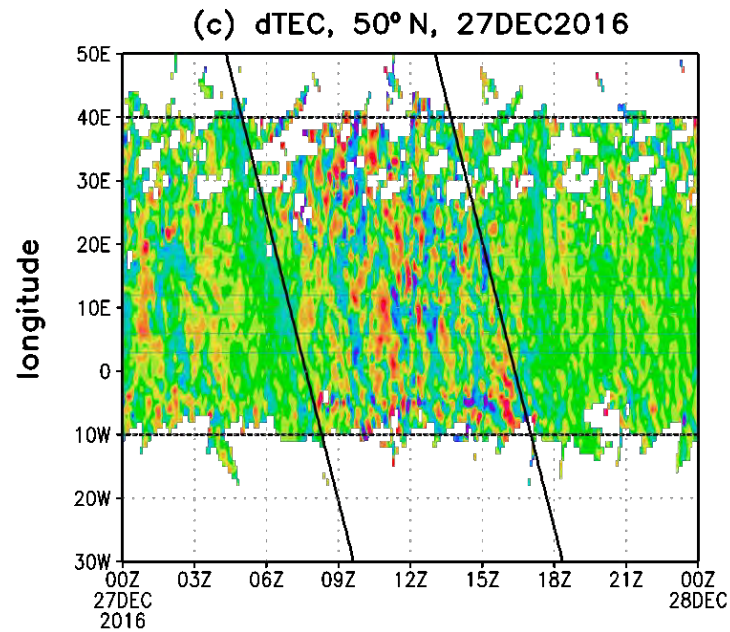
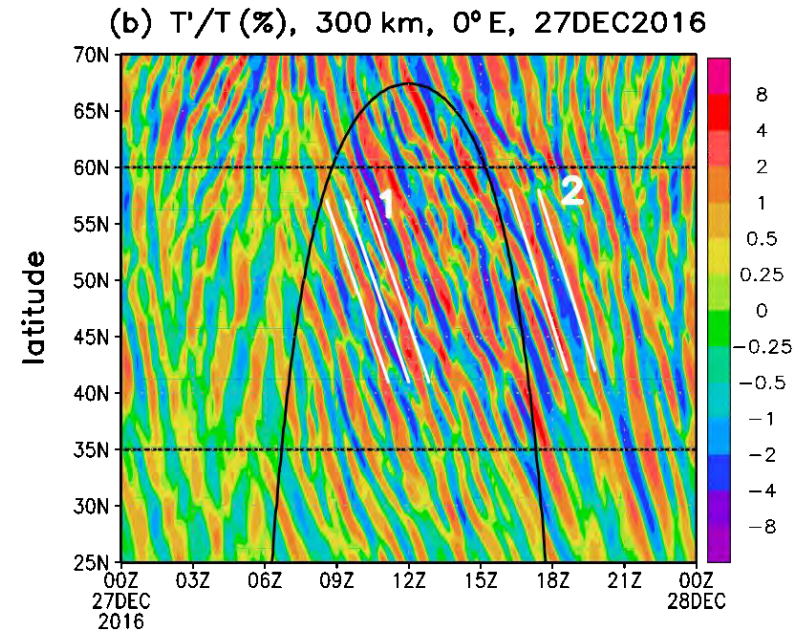
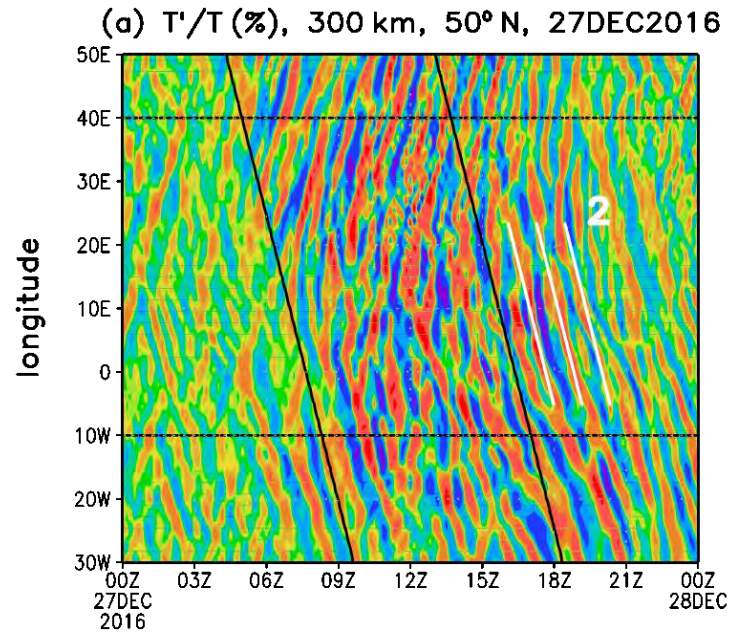
→
250

Maximum GW activity at middle latitudes during local time noon / early afternoon with predo-minantly equatorward propagation.

Additional GW activity at polar latitudes during local time morning with a significant eastward propagation component (the westward tidal flow in this regime is caused by the asymmetry of the auroral circulation between dawn and dusk).

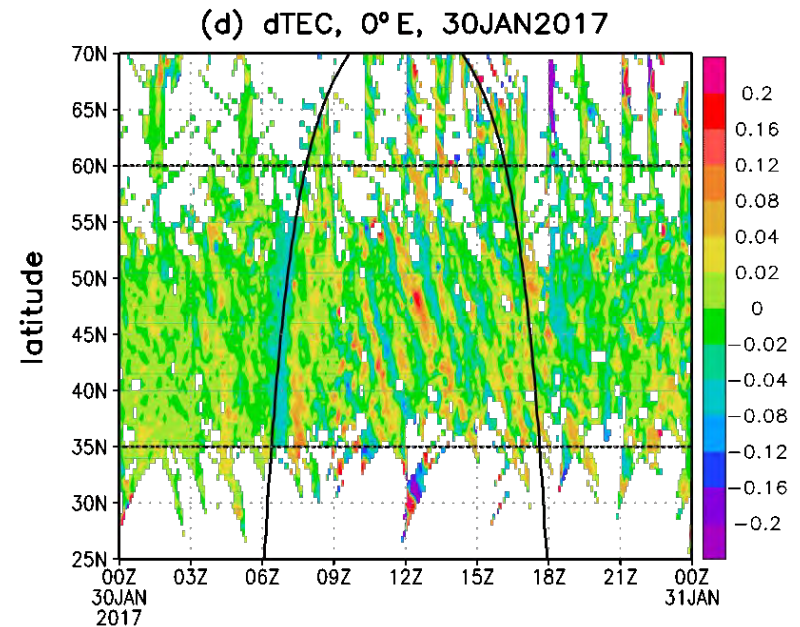
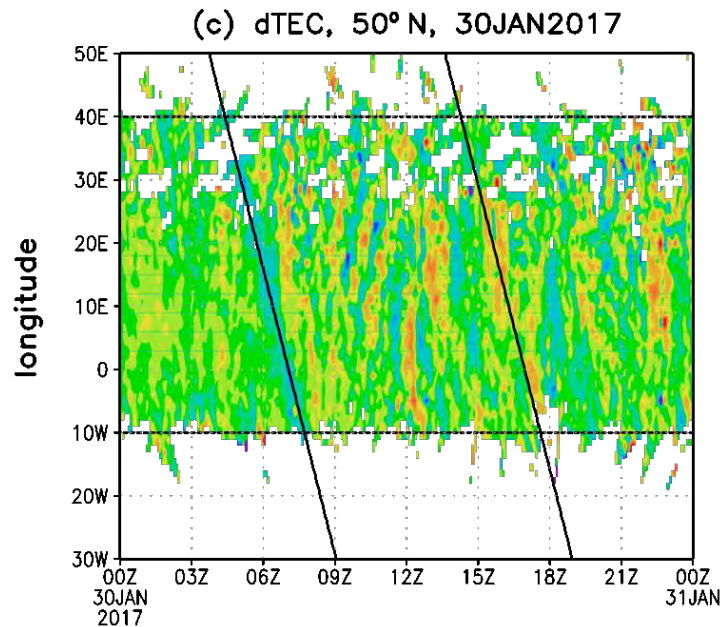
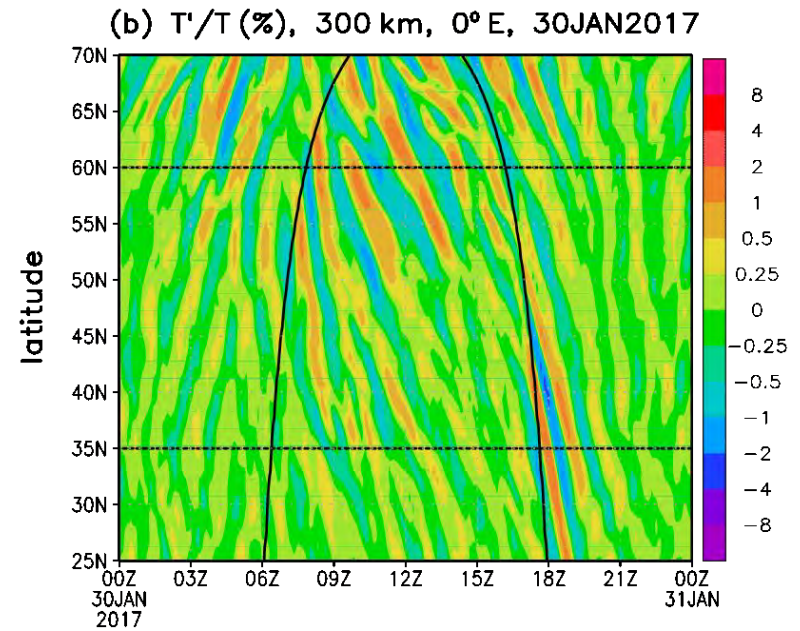
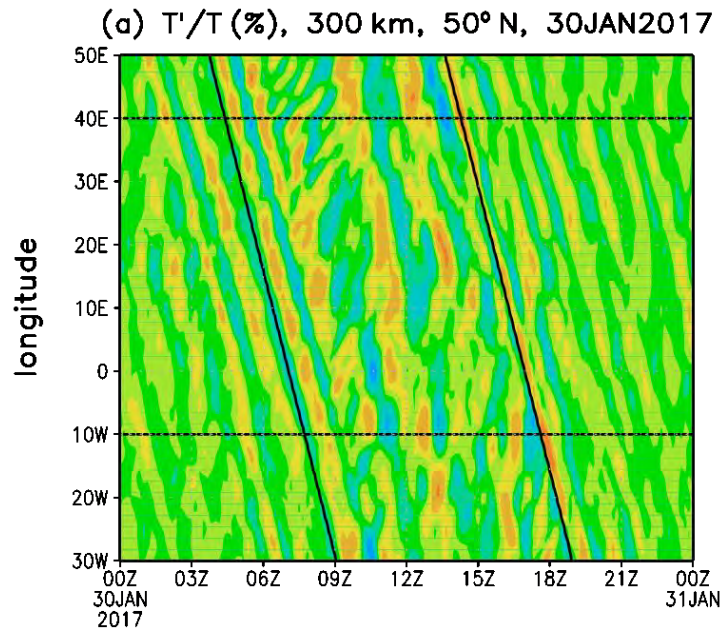
(Becker et al., JGR-SP, 2022)

Thermospheric GWs and GNSS TEC perturbations (Europe, 27DEC2017)



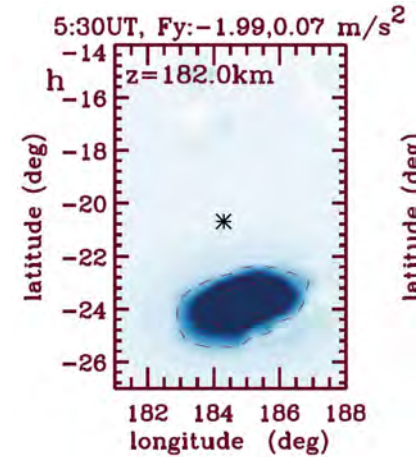
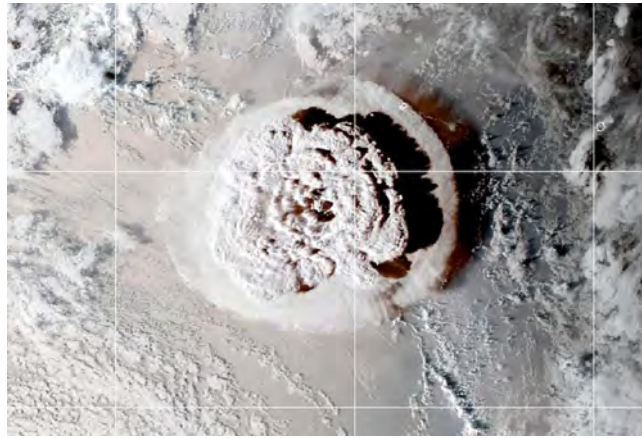
(Becker, Goncharenko, et al., JGR-SP, 2022)

Thermospheric GWs and GNSS TEC perturbations (Europe, 30JAN2017)

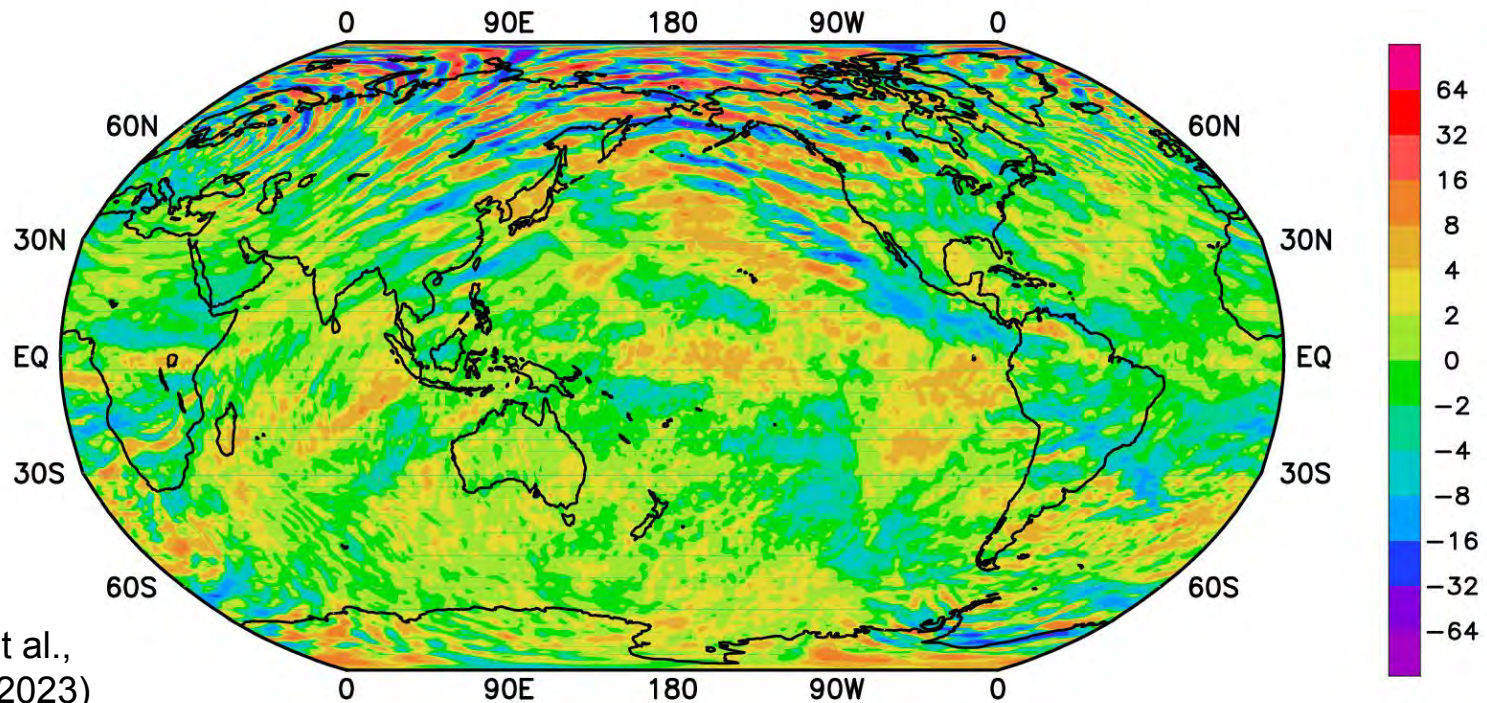


(Becker, Goncharenko, et al., JGR-SP, 2022)

MESORAC-HIAMCM simulation of the response to the Tonga eruption

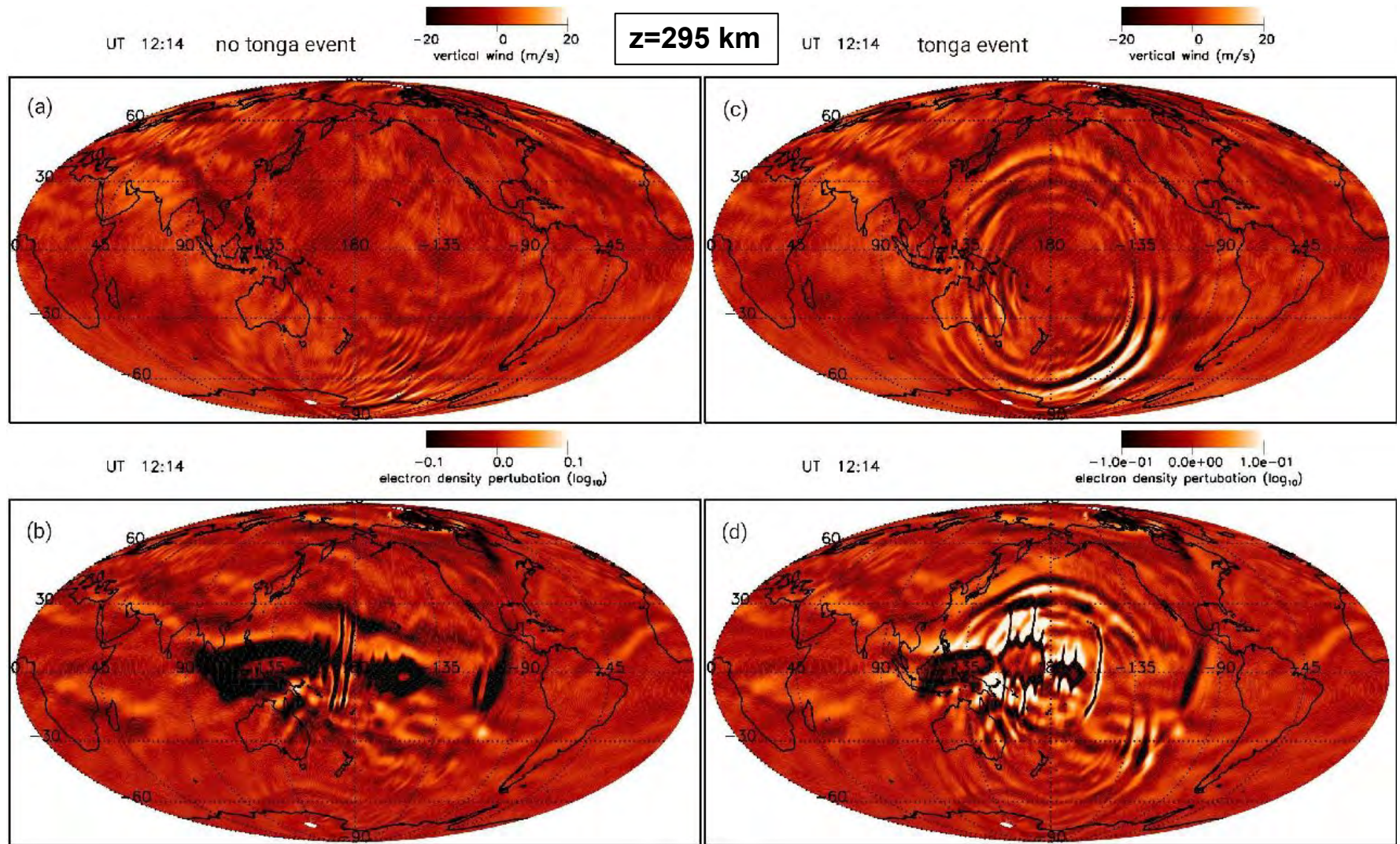


vertical wind (ms^{-1}) at 280 km, 15 JAN 2022, 03:00 UT



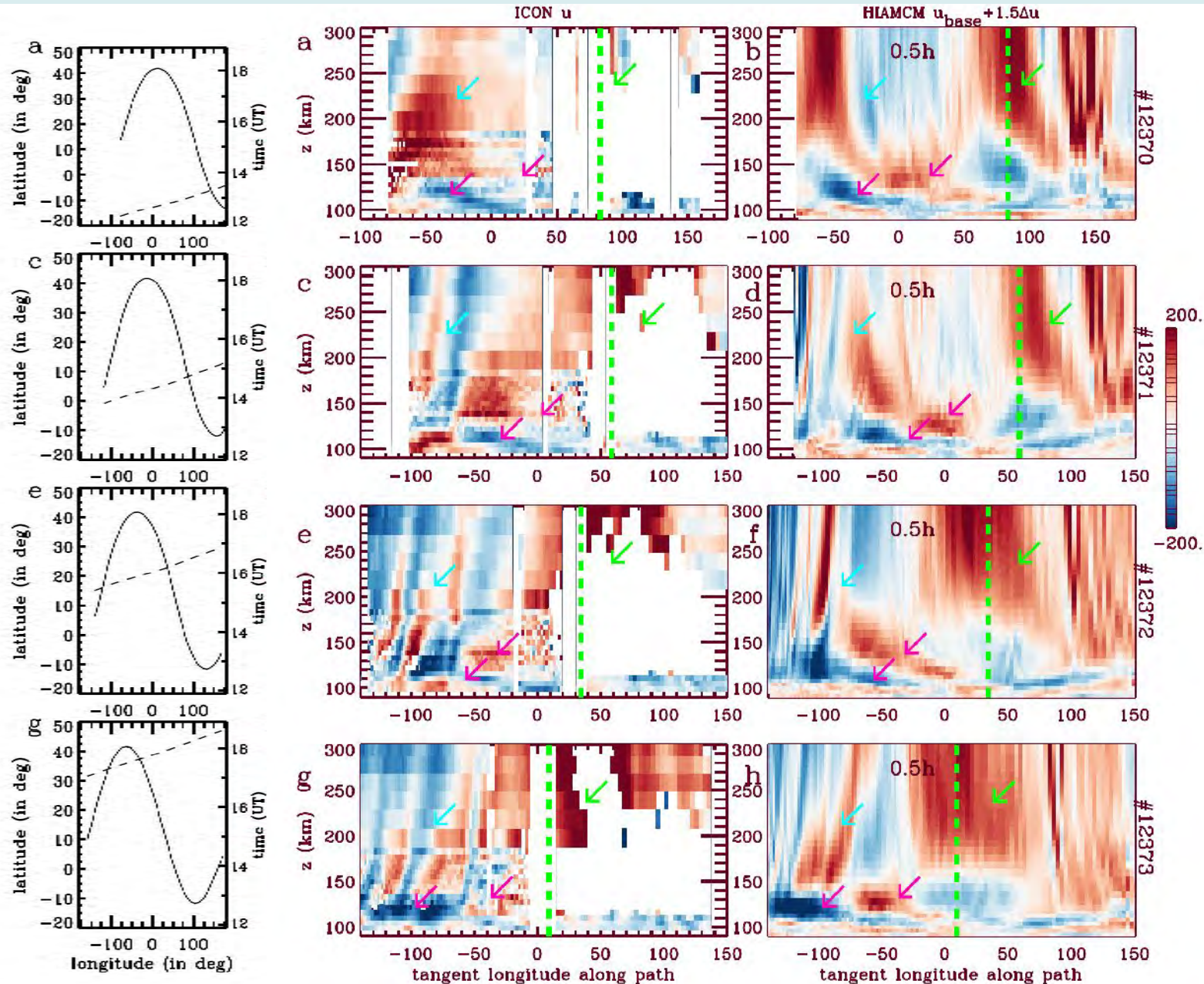
(Vadas et al.,
JGRSP, 2023)

MESORAC-HIAMCM-SAMI3 without and with the Tonga eruption



- concentric ring structures of electron density variations (bottom right) that coincide with the neutral vertical wind variations caused by the Tonga eruption (top right)
- equatorial plasma bubbles (EPBs) over the western Pacific more intense for the eruption case

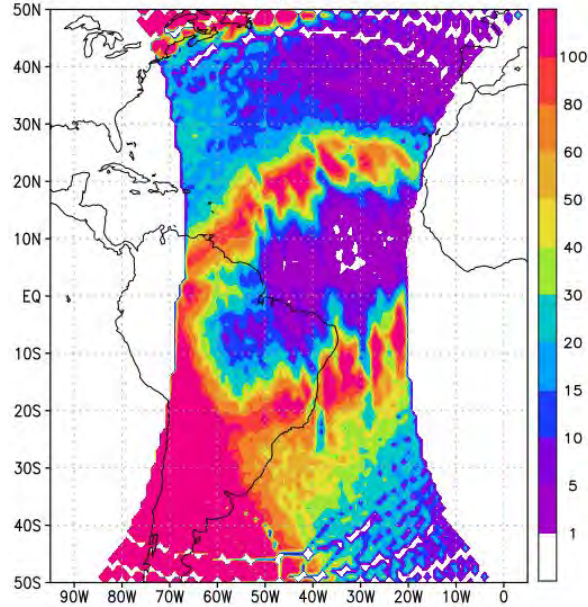
Secondary GWs induced by the Tonga event as observed by ICON-MIGHTI and simulated by MESORAC-HIAMCM



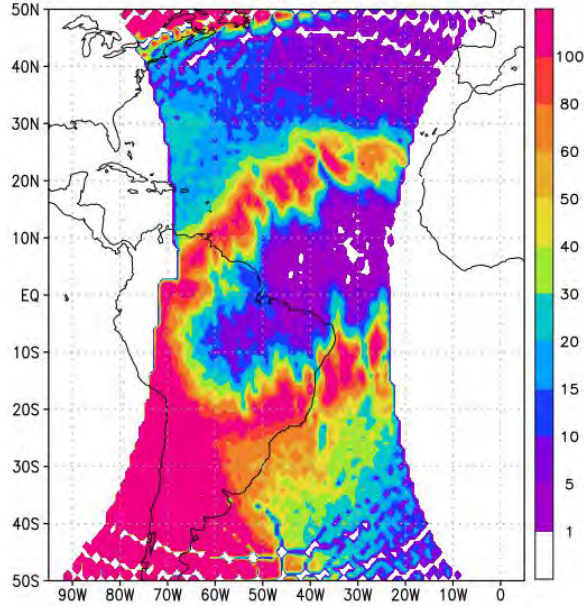
(Vadas et al., JGRSP, 2023)

GOLD L1C data on 14 January 2022

135.6 nm radiance (R), 14JAN2022, 23:10 UT

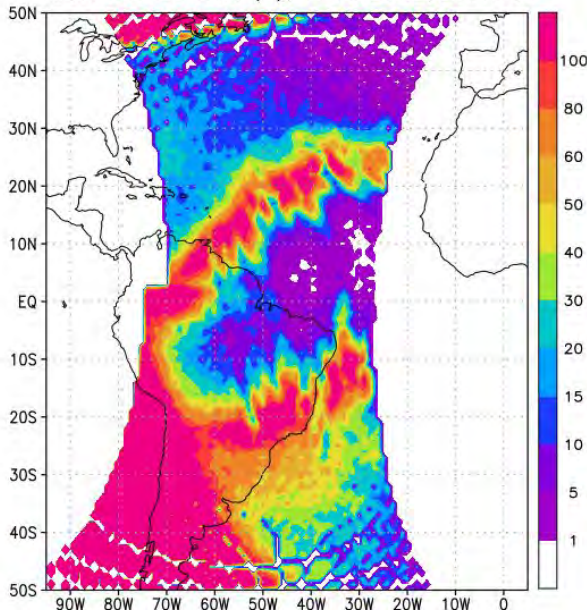


135.6 nm radiance (R), 14JAN2022, 23:25 UT

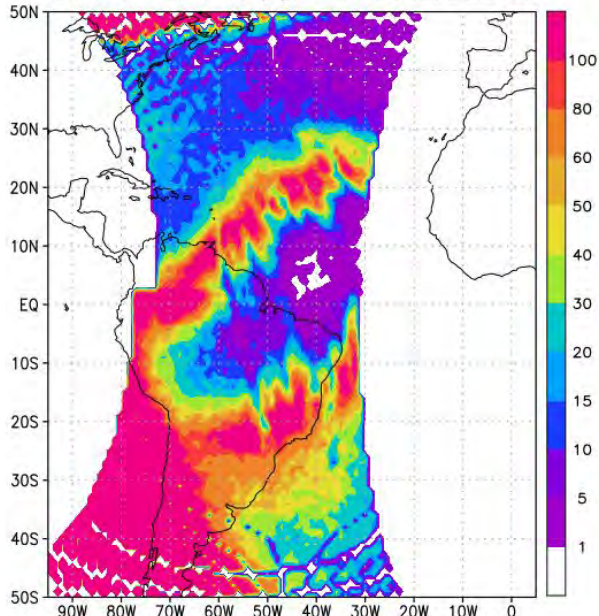


- Regular EIA
- Stronger emission due to geomagnetic storm activity that started on this day.

135.6 nm radiance (R), 14JAN2022, 23:40 UT

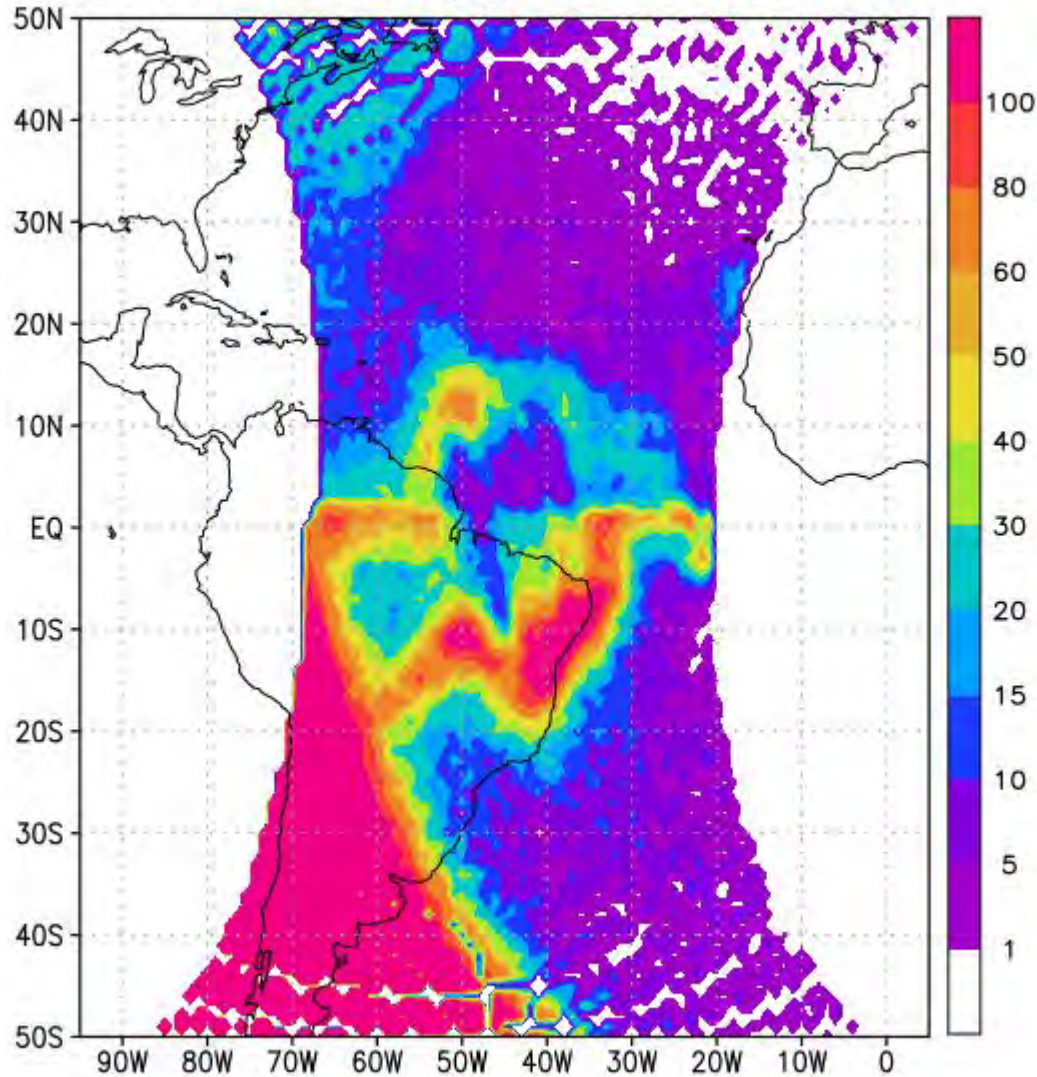


135.6 nm radiance (R), 14JAN2022, 23:55 UT

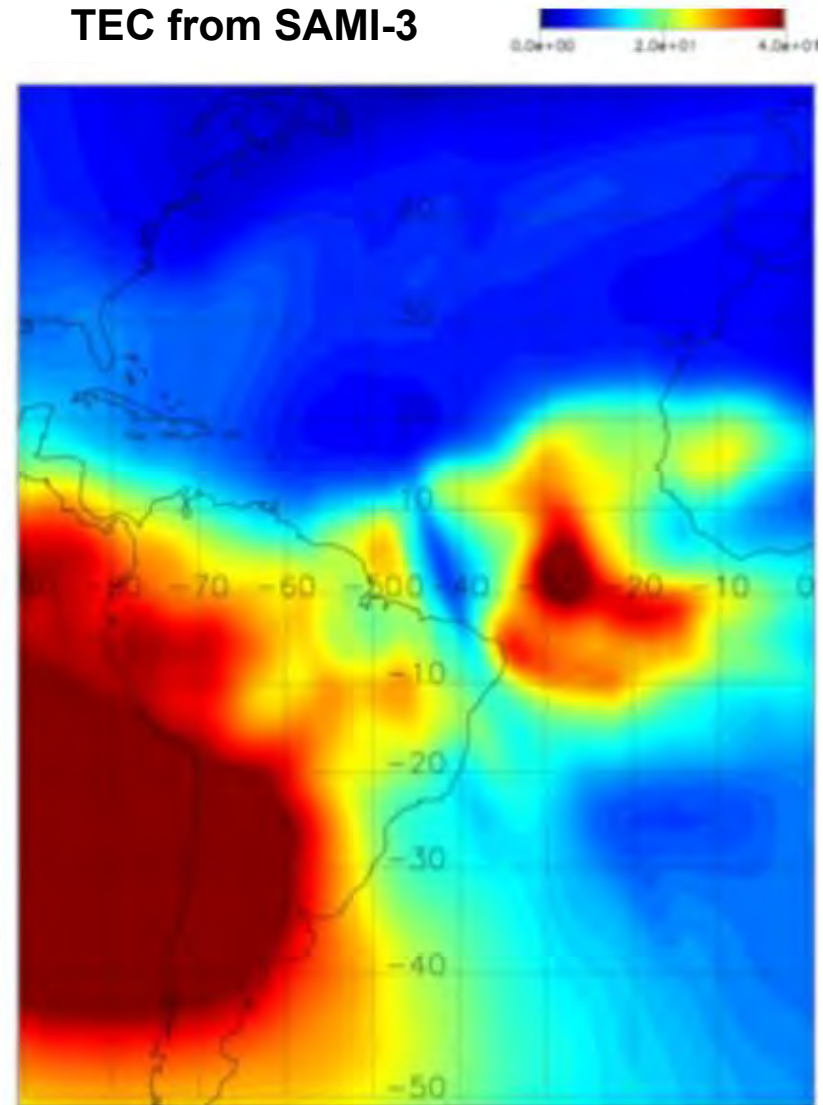


GOLD L1C data versus MEOSRAC-HIAMCM-SAMI3 on 15 January 2022, 23:10 UT

135.6 nm radiance (R), 15JAN2022, 23:10 UT

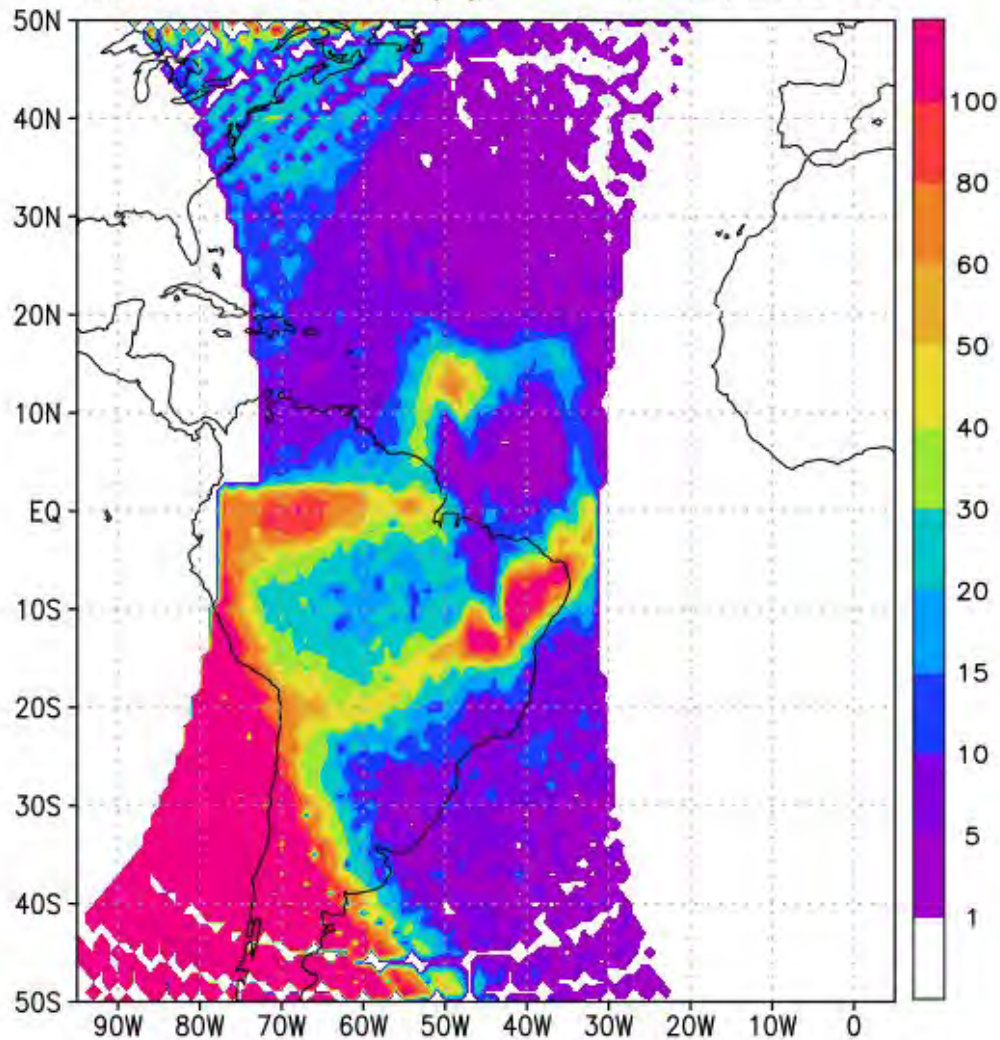


TEC from SAMI-3

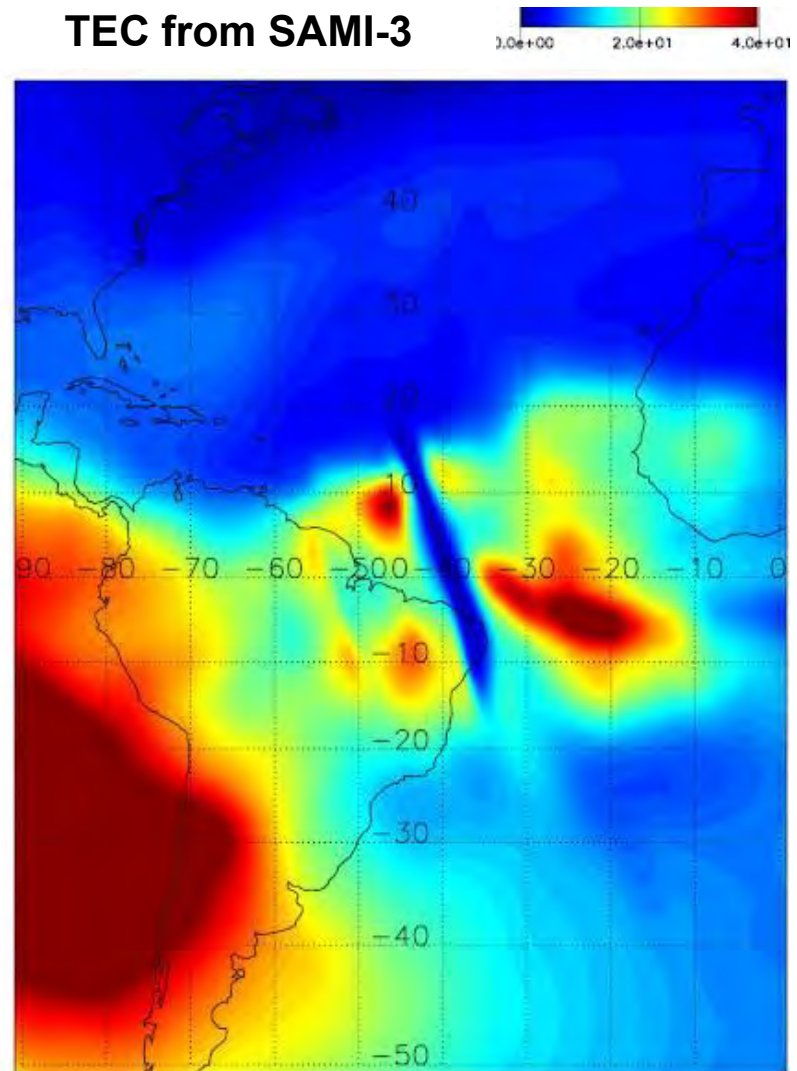


GOLD L1C data versus MEOSRAC-HIAMCM-SAMI3 on 15 January 2022, 23:55 UT

135.6 nm radiance (R), 15JAN2022, 23:55 UT



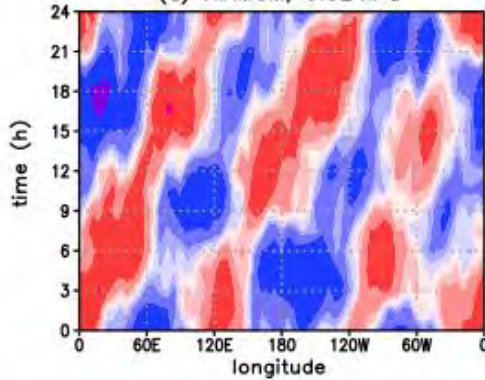
TEC from SAMI-3



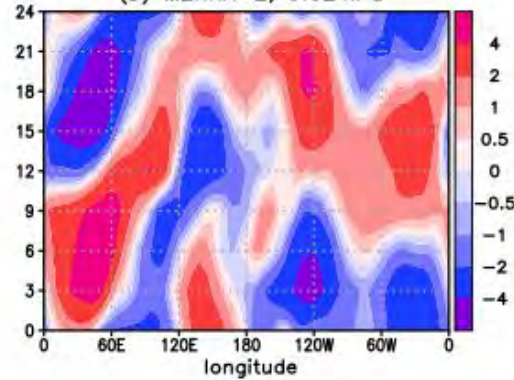
Unexpected DE3 in the southern summer mesosphere

T-tide (K), 1–20JAN2017, 55S

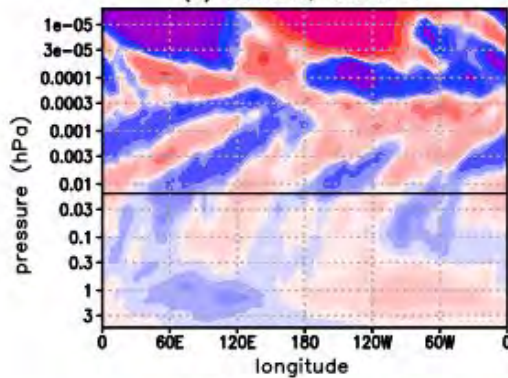
(a) HIAMCM, 0.02 hPa



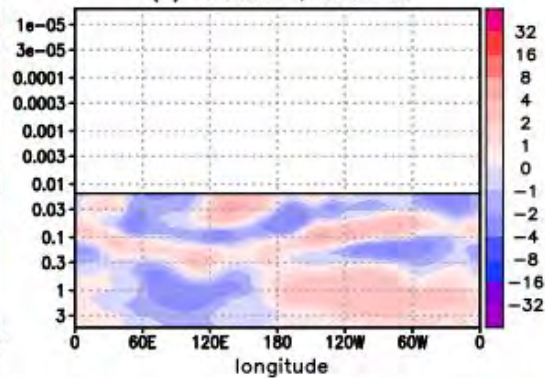
(b) MERRA-2, 0.02 hPa



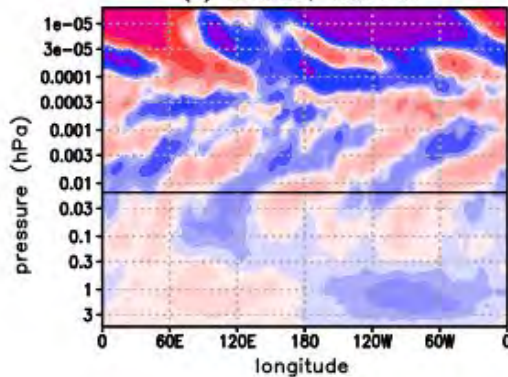
(c) HIAMCM, 00:00 UT



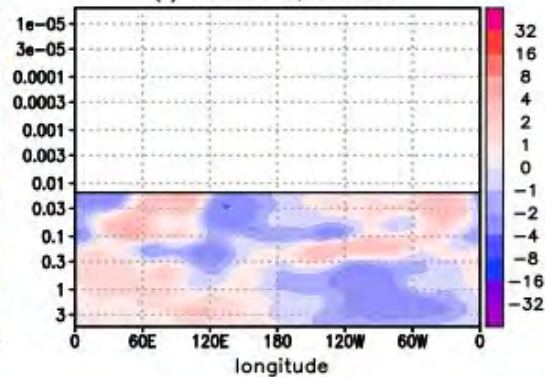
(d) MERRA-2, 00:00 UT



(e) HIAMCM, 12:00 UT



(f) MERRA-2, 12:00 UT

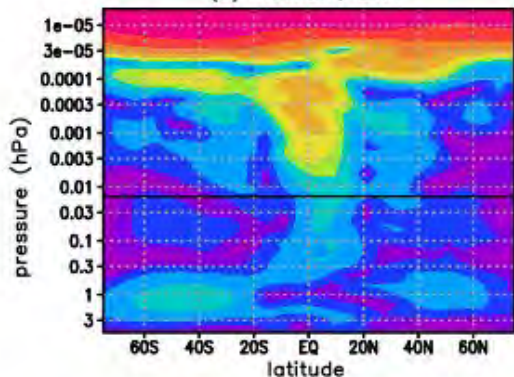


- Conventional wisdom based on linear theory/models and conventional WAMs with parameterized GWs: DW1 tide extends somewhat into the summer mesosphere.
- A diurnal tide in the mesosphere is usually found in observations.
- The HIAMCM indicates a **predominant DE3** (instead of a DW1) in the **southern summer mesosphere**.
- This is confirmed by MERRA-2 and SABER (not shown).

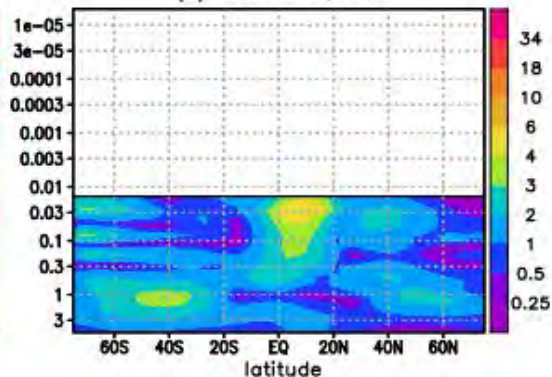
Unexpected DE3 in the southern summer mesosphere

tidal T-amplitudes (K), 1–20JAN2017

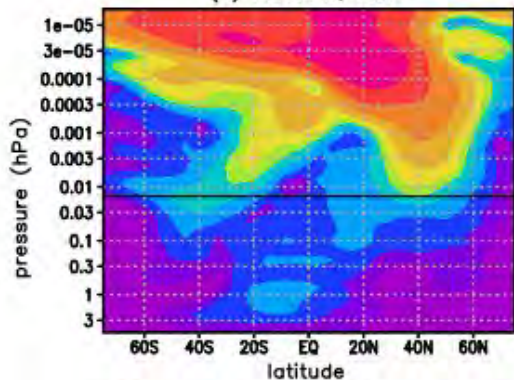
(a) HIAMCM, DW1



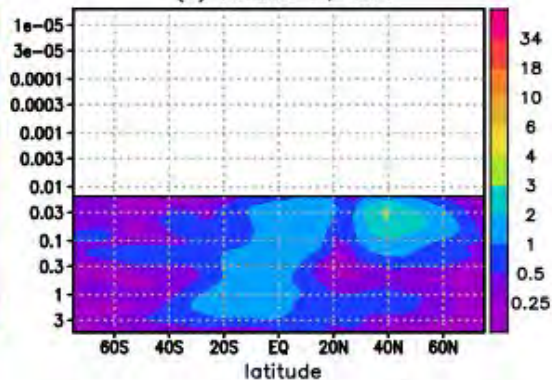
(b) MERRA-2, DW1



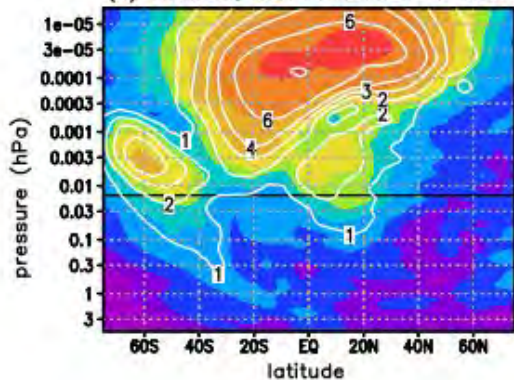
(c) HIAMCM, SW2



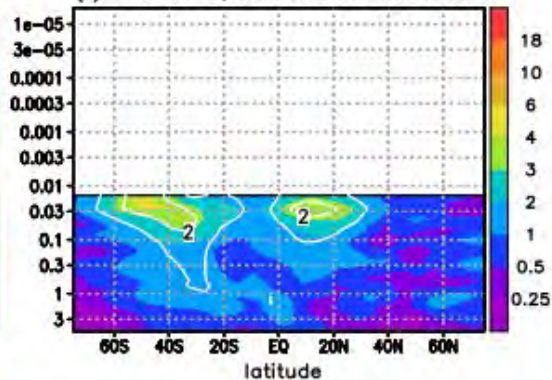
(d) MERRA-2, SW2



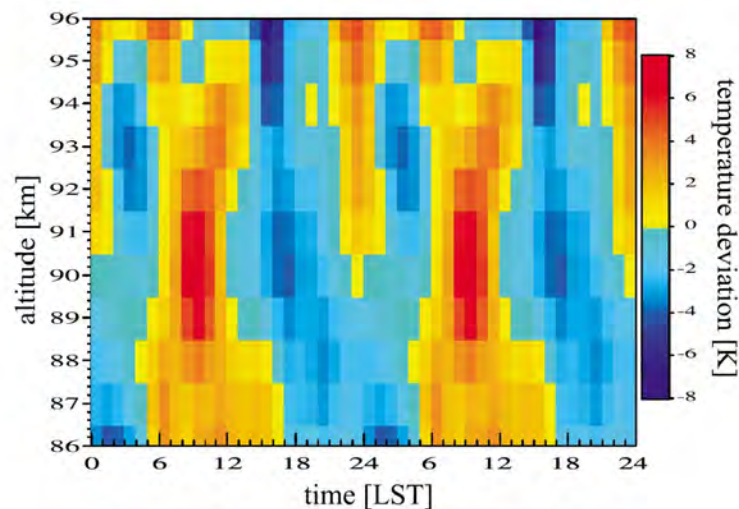
(e) HIAMCM, DE1+DE2+DE3 & DE3



(f) MERRA-2, DE1+DE2+DE3 & DE3



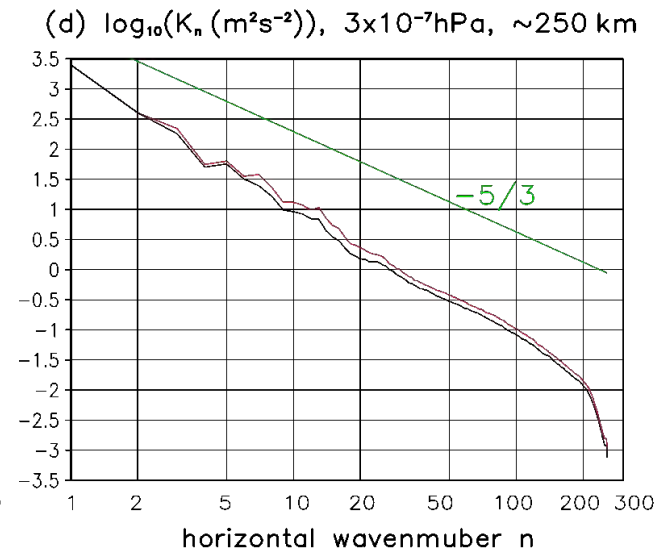
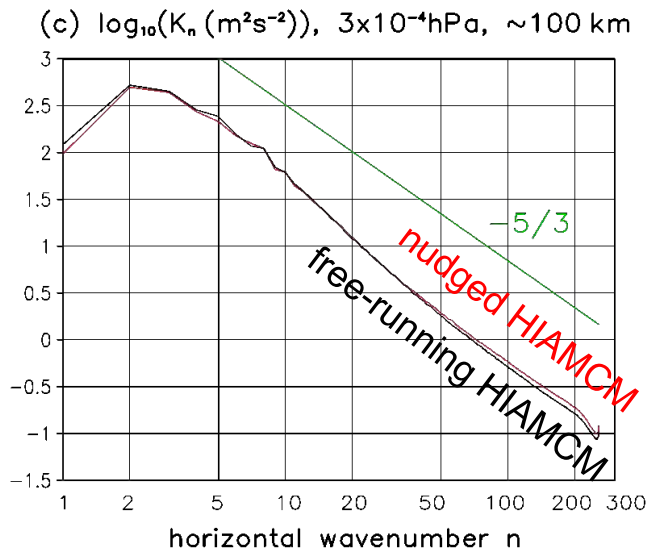
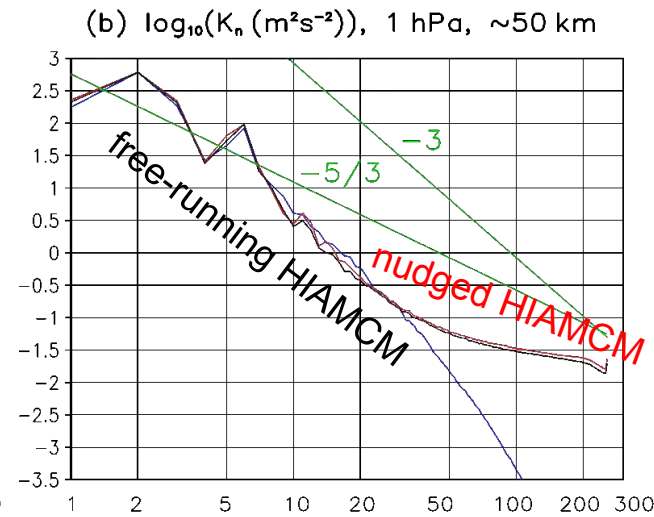
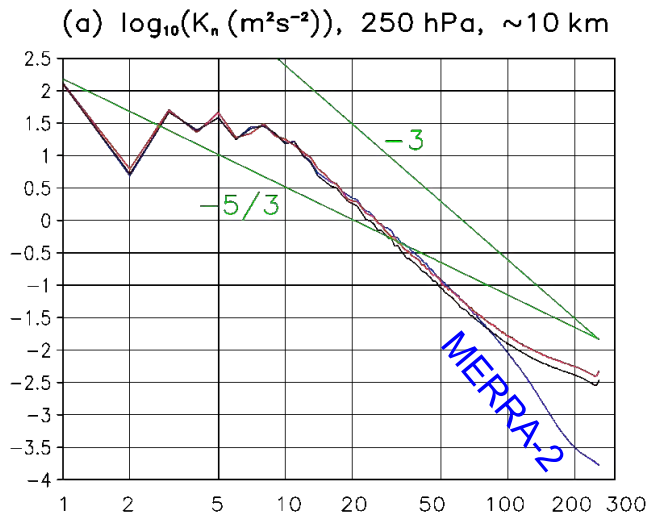
Average daily cycle of T' (K) in January 2011 as observed by lidar at Davis (Antarctica) (Lübken et al, 2011, GRL)



Summary

- **A GW-resolving GCM requires not only sufficiently high numerical resolution, but also a physics-based macro-turbulent diffusion scheme** (Classical Smagorinsky Model routinely used in the HIAMCM).
- Secondary and higher-order GWs are essential to understand the GW activity and the large-scale flow in the winter middle and upper atmosphere.
- Higher-order GWs in the winter thermosphere show propagation characteristics similar to observed quiet-time TEC perturbations.
- GW-mean flow interaction in the thermosphere means GW-tidal interaction.
- Simulation of the GW response to the Tonga eruption is possible when we first compute the primary GWs and their ambient-flow effects using MESORAC.
- The resulting secondary GWs in HIAMCM have very large amplitudes ($w' > 50$ m/s), very large phase speeds (up to 700 m/s), and medium to large horizontal scales. These waves agree well with satellite measurements.
- MESORAC-HIAMCM-SAMI3 simulation of the Tonga event: Very strong equatorial plasma bubbles over the Pacific; intersection of the EIA crests over the Atlantic sector as observed by GOLD.
- GW-tidal interactions may be crucial for explaining the unexpected DE3 tide in the southern summer mesosphere.
- **Outlook: Higher resolution: Dynamical Smagorinsky Model**

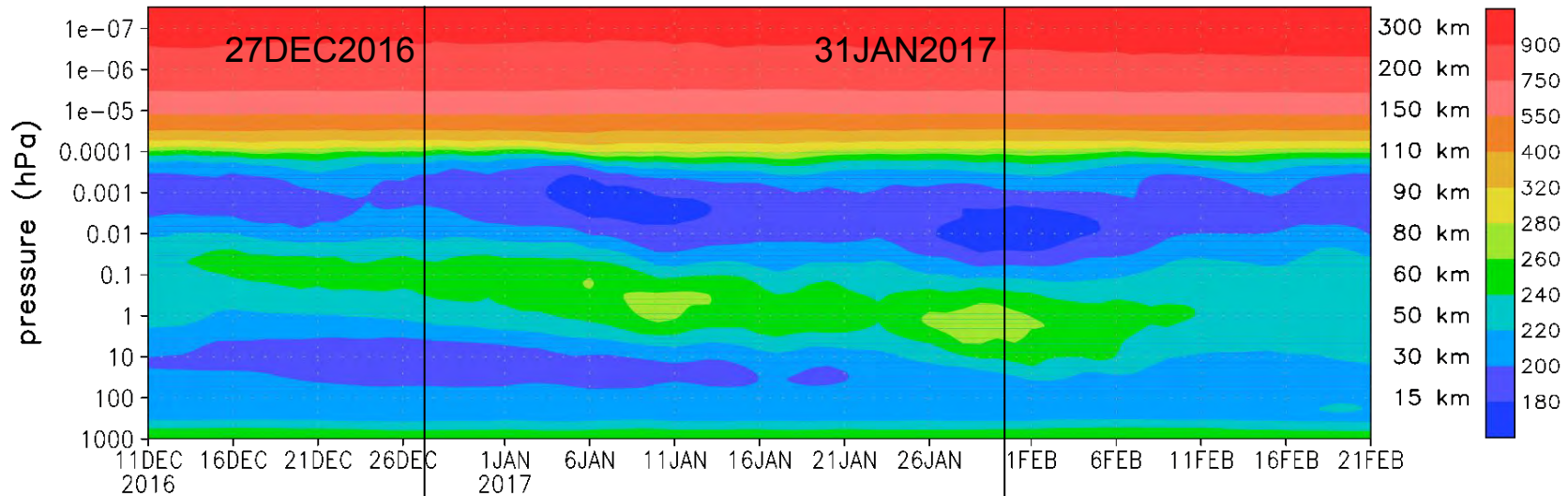
Global kinetic energy spectra (January 2016)



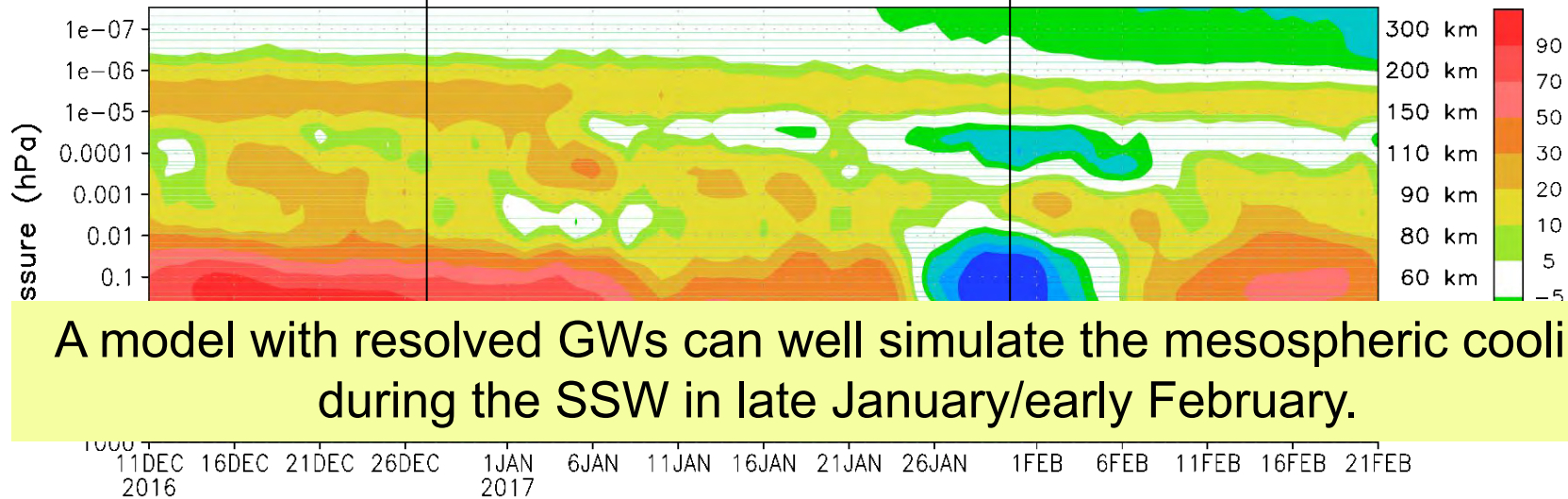
- The nudged and the free-running HIAMCM simulate roughly the same energy spectra and capture the Nastrom-Gage spectrum in upper troposphere.
- Shallow spectra in the stratosphere (presumably because inertia GWs are damped due to short λ_z).
- Broad range of a $-5/3$ exponential spectral slope in the mesopause region: Macro turbulence with a forward energy cascade like in the upper troposphere?
- MERRA-2 dramatically underestimates the energy in the mesoscales for $\lambda_h < 400 \text{ km}$ in the troposphere and for $\lambda_h < 1500 \text{ km}$ in the upper stratosphere.
- Steeper spectra in the thermosphere because of molecular viscosity.

Mean fields during the winter 2016/2017 from a GW-resolving WAM nudged to MERRA-2 reanalysis

(a) temperature (K), 70°N–90°N



(b) zonal wind (ms^{-1}), 50°N–70°N



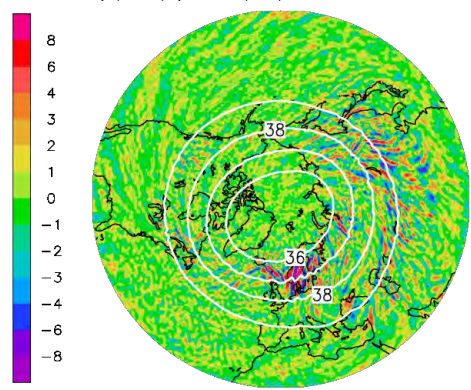
A model with resolved GWs can well simulate the mesospheric cooling during the SSW in late January/early February.

GWs and large-scale flow from the stratosphere to the thermosphere for strong vortex: 27DEC2016

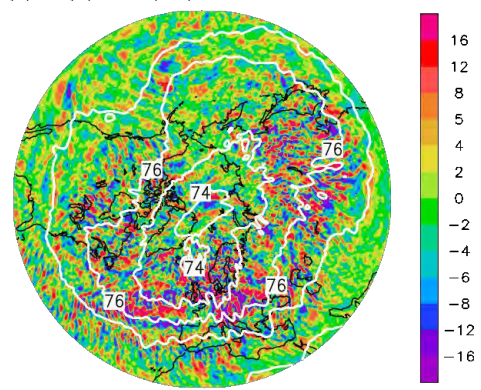
- Primary GWs in the stratosphere (3 hPa, generated presumably in the upper troposphere) are strongest over Scandinavia.
- The GW activity (primary and secondary) spreads out in the mesosphere.
- Two major sources of tertiary GWs in the lower thermosphere over northern Europe and eastern Siberia (concentric ring structures at 150 km).
- Only the tertiary GWs that propagate against the mean flow associated with the diurnal tide (white arrows) propagate to higher altitudes, leading to partial concentric ring structures at 250 km.

SNAPSHOTS ON 27 DECEMBER 2016

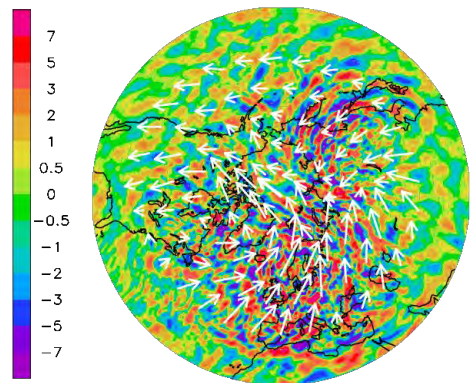
(a) T' (K) & z (km), 3 hPa, 12:00 UT



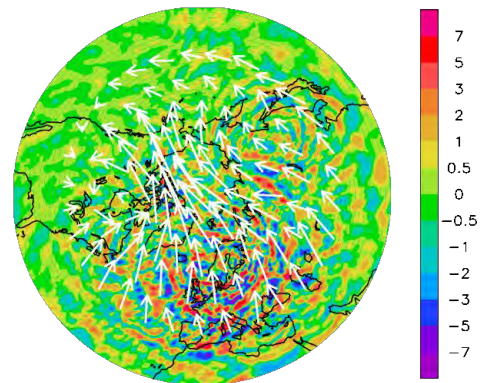
(b) T' (K) & z (km), 0.01 hPa, 12:00 UT



(c) T'/T (%) & (U,V) (ms^{-1}), 150 km, 12:00 UT

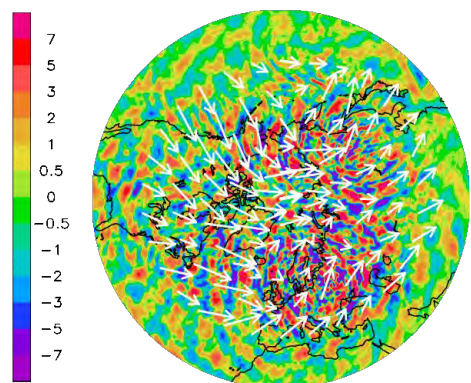


(d) T'/T (%) & (U,V) (ms^{-1}), 250 km, 12:00 UT

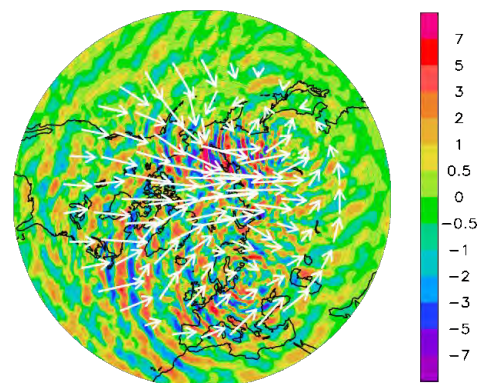


→
160

(e) T'/T (%) & (U,V) (ms^{-1}), 150 km, 19:30 UT

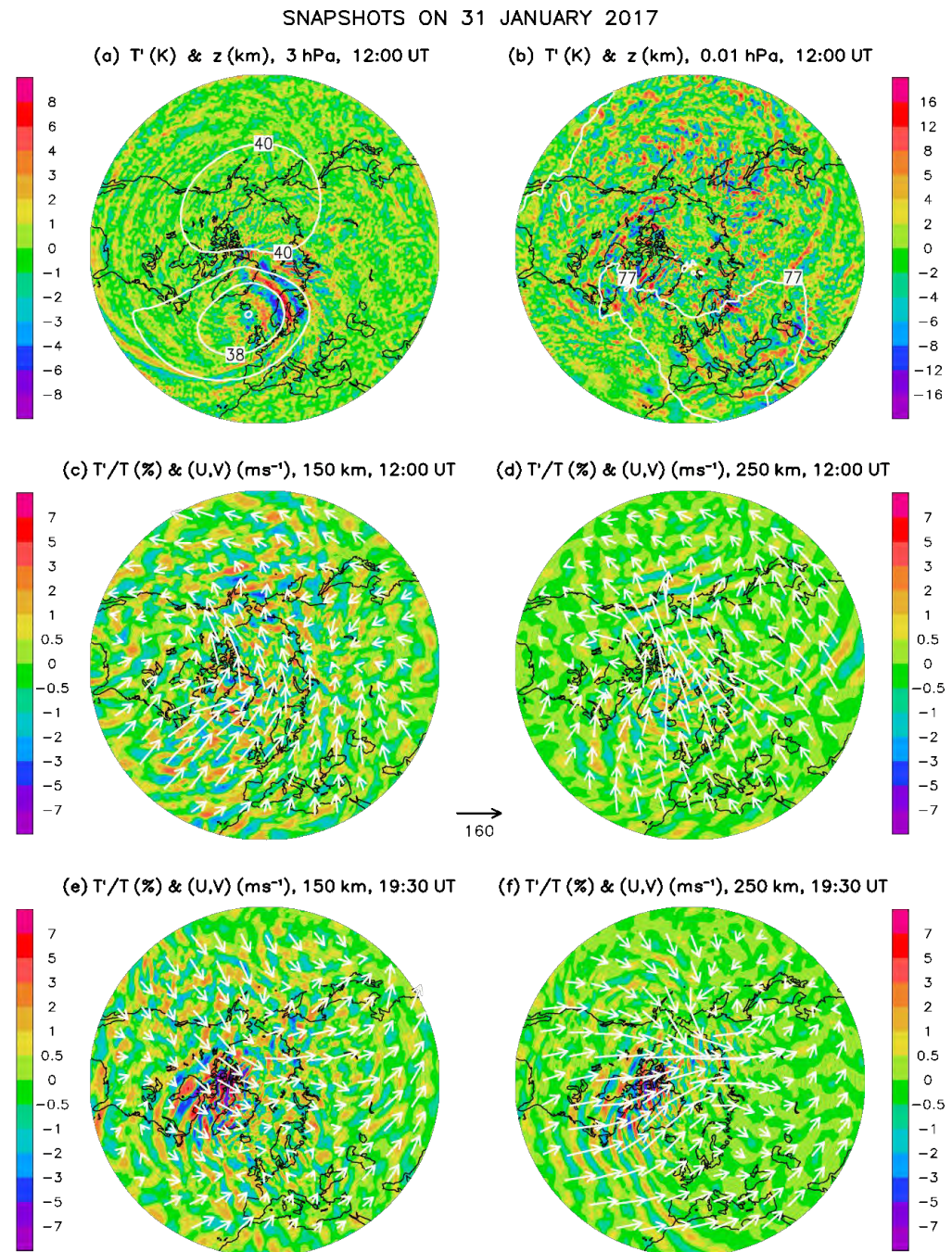


(f) T'/T (%) & (U,V) (ms^{-1}), 250 km, 19:30 UT



GWs and large-scale flow from the stratosphere to the thermosphere during the SSW: 31JAN2017

- Weaker GW activity at all altitudes when compared to the strong-vortex period.
- Weakening effect of GWs in the thermosphere is stronger over Europe than over North America (for this particular event).



Hydrodynamically consistent framework for macro-turbulent and molecular diffusion (as well as ion drag) in GCMs

(Becker, JAS, 2017; Becker & Vadas, 2020)

$$(\partial_t \mathbf{v})_{diff} = \rho^{-1} \nabla_h (\rho (K_h + \nu_h) S_h) + \rho^{-1} \partial_z (\rho (K_z + \nu_z) \partial_z \mathbf{v})$$

$$S_h = \{(\nabla + \mathbf{e}_z/a) \circ \mathbf{v}\} + \{(\nabla + \mathbf{e}_z/a) \circ \mathbf{v}\}^T - 1 \nabla \cdot \mathbf{v}$$

$$\begin{aligned} c_p (\partial_t T)_{diff} &= \frac{c_p}{\rho} \nabla_h \left(\rho \frac{K_h + \nu_h}{0.7} \nabla_h T \right) \\ &+ \frac{c_p}{\rho} \partial_z \left(\rho \left(\frac{K_z}{Pr} (g/c_p + \partial_z T) + \frac{\nu_z}{0.7} \partial_z T \right) \right) \\ &+ \underbrace{(K_h + \nu_h) |S_h|^2}_{\epsilon_h} + \underbrace{(K_z + \nu_z) (\partial_z \mathbf{v})^2}_{\epsilon_z} \end{aligned}$$

$\nu \sim \nu_h \sim \nu_z \sim K_h \gg K_z$ surface to lower thermosphere
 $\nu \sim \nu_h \sim \nu_z \sim K_h \gg K_z$ middle thermosphere
 $\nu \sim \nu_h > \nu_z \gg K_h \gg K_z$ upper thermosphere

$$\begin{aligned} (\partial_t \mathbf{v})_{ion\ drag} &= D \mathbf{v} \\ c_p (\partial_t T)_{ion\ drag} &= -\mathbf{v} \cdot (D \mathbf{v}) = \epsilon_{ion\ drag} \end{aligned}$$

Classical Smagorinsky Model (CSM) for macro-turbulent diffusion

(Becker & Burkhardt, MWR-2007, Becker, JAS-2009)

$$K_h = l_h^2 |S_h| (1 + \alpha F(R_i)) \gg K_z = l_z^2 |\partial_z \mathbf{v}| F(R_i)$$

$$F(R_i) = \begin{cases} \sqrt{1 - 18 R_i} & R_i < 0 \\ (1 + 9 R_i)^{-1}, & R_i \geq 0 \end{cases}$$

$$R_i = N^2 / (\partial_z \mathbf{v})^2 \rightarrow R_i - \frac{1}{4} \quad \text{for } p < 100 \text{ hPa}$$

$$P_r = \max(1, R_i) \quad \text{since}$$

$$0 \leq \epsilon_{mech} = K_h |S_h|^2 + K_z (\partial_z \mathbf{v})^2 - \frac{K_z}{P_r} N^2$$

Molecular viscosity in the thermosphere

(e.g., Vadas, 2007, JGR; Vadas & Crowley, 2017, JGR; Becker & Vadas, JGR-SP, 2020)

$$\nu = 3.34 \times 10^{-7} \left(\frac{T}{\text{K}} \right)^{1.71} \left(\frac{R}{\text{J/K}} \right) \left(\frac{p}{\text{Pa}} \right)^{-1} \text{ m}^2 \text{ s}^{-1}$$

$$\nu_z = \left(\nu^{-1} + \nu_{z \max}^{-1} \right)^{-1}, \quad \nu_{z \max} = 3.5 \times 10^6 \text{ m}^2 \text{ s}^{-1}$$

$$\nu_h = \left(\nu^{-1} + \nu_{h \max}^{-1} \right)^{-1}, \quad \nu_{h \max} = 7.1 \times 10^7 \text{ m}^2 \text{ s}^{-1}$$

Classical Smagorinsky Model (CSM) for macro-turbulent diffusion

(Becker & Burkhardt, MWR-2007, Becker, JAS-2009)

$$K_h = l_h^2 |S_h| (1 + \alpha F(R_i)) \gg K_z = l_z^2 |\partial_z \mathbf{v}| F(R_i)$$

$$F(R_i) = \begin{cases} \sqrt{1 - 18 R_i} & R_i < 0 \\ (1 + 9 R_i)^{-1}, & R_i \geq 0 \end{cases}$$

$$R_i = N^2 / (\partial_z \mathbf{v})^2 \rightarrow R_i - \frac{1}{4} \text{ for } p < 100 \text{ hPa}$$

$$P_r = \max(1, R_i) \text{ since}$$

$$0 \leq \epsilon_{mech} = K_h |S_h|^2 + K_z (\partial_z \mathbf{v})^2 - \frac{K_z}{P_r} N^2$$

Molecular viscosity in the thermosphere

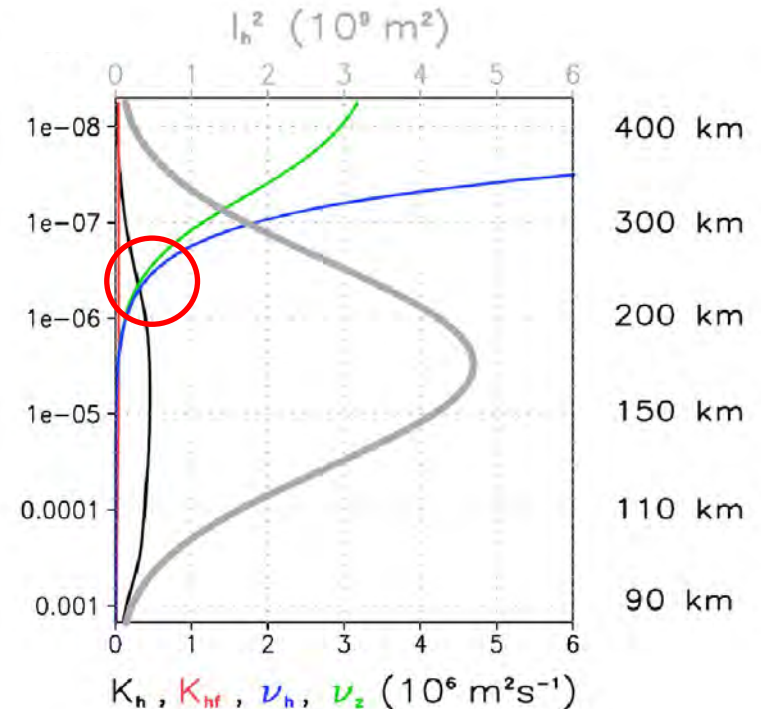
(e.g., Vadas, 2007, JGR; Vadas & Crowley, 2017, JGR; Becker & Vadas, JGR-SP, 2020)

$$\nu = 3.34 \times 10^{-7} \left(\frac{T}{\text{K}}\right)^{1.71} \left(\frac{R}{\text{J/K}}\right) \left(\frac{p}{\text{Pa}}\right)^{-1} \text{ m}^2 \text{ s}^{-1}$$

$$\nu_z = \left(\nu^{-1} + \nu_{z \max}^{-1}\right)^{-1}, \quad \nu_{z \max} = 3.5 \times 10^6 \text{ m}^2 \text{ s}^{-1}$$

$$\nu_h = \left(\nu^{-1} + \nu_{h \max}^{-1}\right)^{-1}, \quad \nu_{h \max} = 7.1 \times 10^7 \text{ m}^2 \text{ s}^{-1}$$

Global-mean profiles: Molecular viscosity exceeds macro-turbulent viscosity above ~200-250 km → **DNS in the F-region.**



Consistent thermodynamics with sensible heat as prognostic variable

(Becker & Vadas, 2020)

one component: $h = c_p T$, $p/\rho = RT$, $dh = c_p dT = \rho^{-1} dp + T ds$

many components: $h_n = c_{pn} T$, $p_n/\rho_n = R_n T$, $dh_n = c_{pn} dT = \rho_n^{-1} dp_n + T ds_n$

$$\rho = \sum_n \rho_n, \quad p = \sum_n p_n, \quad s = \sum_n s_n, \quad q_n = \rho_n/\rho, \quad R = \sum_n q_n R_n, \quad c_p = \sum_n q_n c_{pn}$$

$$\Rightarrow h = \sum_n h_n = c_p T, \quad p/\rho = RT, \quad \text{but: } dh = \rho^{-1} dp + T ds + \sum_n (h_n - T s_n) dq_n$$

extending a GCM into the thermosphere

(one component, but variable R and c_p above the mesopause):

$$dh = T \left(\frac{\partial s}{\partial T} \right)_p dT \quad \text{for } R = R(p)$$

$$dh = T \left(\frac{\partial s}{\partial T} \right)_p dT - \frac{T}{R \rho} \left(\frac{\partial R}{\partial T} \right)_p dp \quad \text{for } R = R(p, T)$$

→ consistency of the thermodynamic equation requires

$$R = R(p) \quad \text{and} \quad c_p = T \left(\frac{\partial s}{\partial T} \right)_p = c_p(T)$$

Consistent thermodynamics with sensible heat as prognostic variable

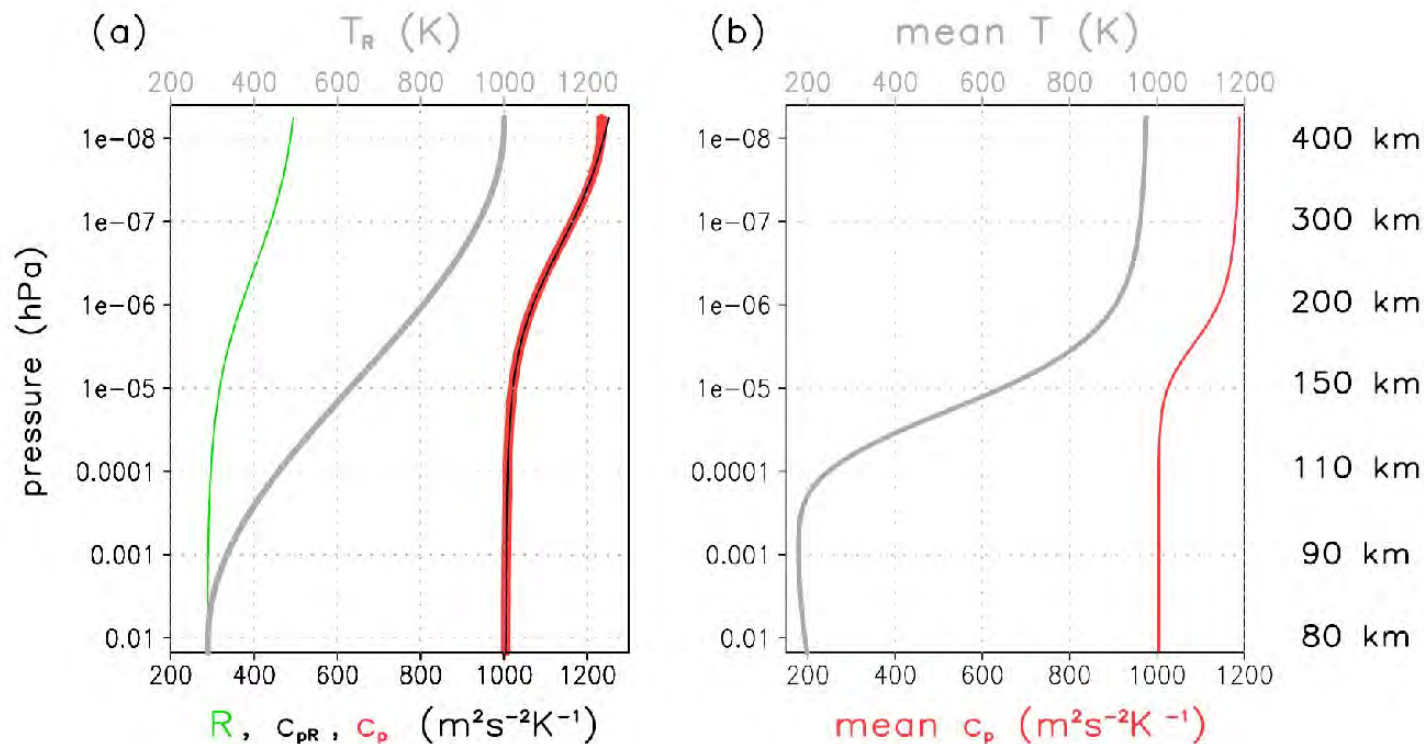
(Decker & Vadas, 2020)

→ consistency of the thermodynamic equation requires

$$R = R(p) \quad \text{and} \quad c_p = T \left(\frac{\partial s}{\partial T} \right)_p = c_p(T)$$

Construction of $R(p)$ and $c_p(T)$:

Use global-mean profiles for $R(p)$, $c_{pR}(p)$, and $T_R(p)$ based on TIME-GCM results for moderate solar maximum conditions; expand c_p into a series of Legendre polynomials; fit coefficients as functions of T_R ; use this expansion to define $c_p(T)$.



Non-hydrostatic correction (middle and upper atmosphere)

(Becker & Vadas, 2020)

$$\partial_t \mathbf{v} = \dots - \nabla \Phi^h - \nabla \Phi^{nh}$$

$$\partial_p \Phi^h = -\frac{RT}{p} \Rightarrow \dot{w} \approx -\partial_p \Phi^{nh} \partial_z p$$

$$w \approx -\frac{RT}{gp} \dot{p}, \quad \dot{p} = -\int_0^p D d\hat{p} \Rightarrow \dot{w} \approx \frac{RT}{gp} \left(\dot{p} D + \int_0^\eta \partial_t D \partial_{\hat{\eta}} p d\hat{\eta} + \mathbf{v} \cdot \int_0^\eta \nabla D \partial_{\hat{\eta}} p d\hat{\eta} \right)$$

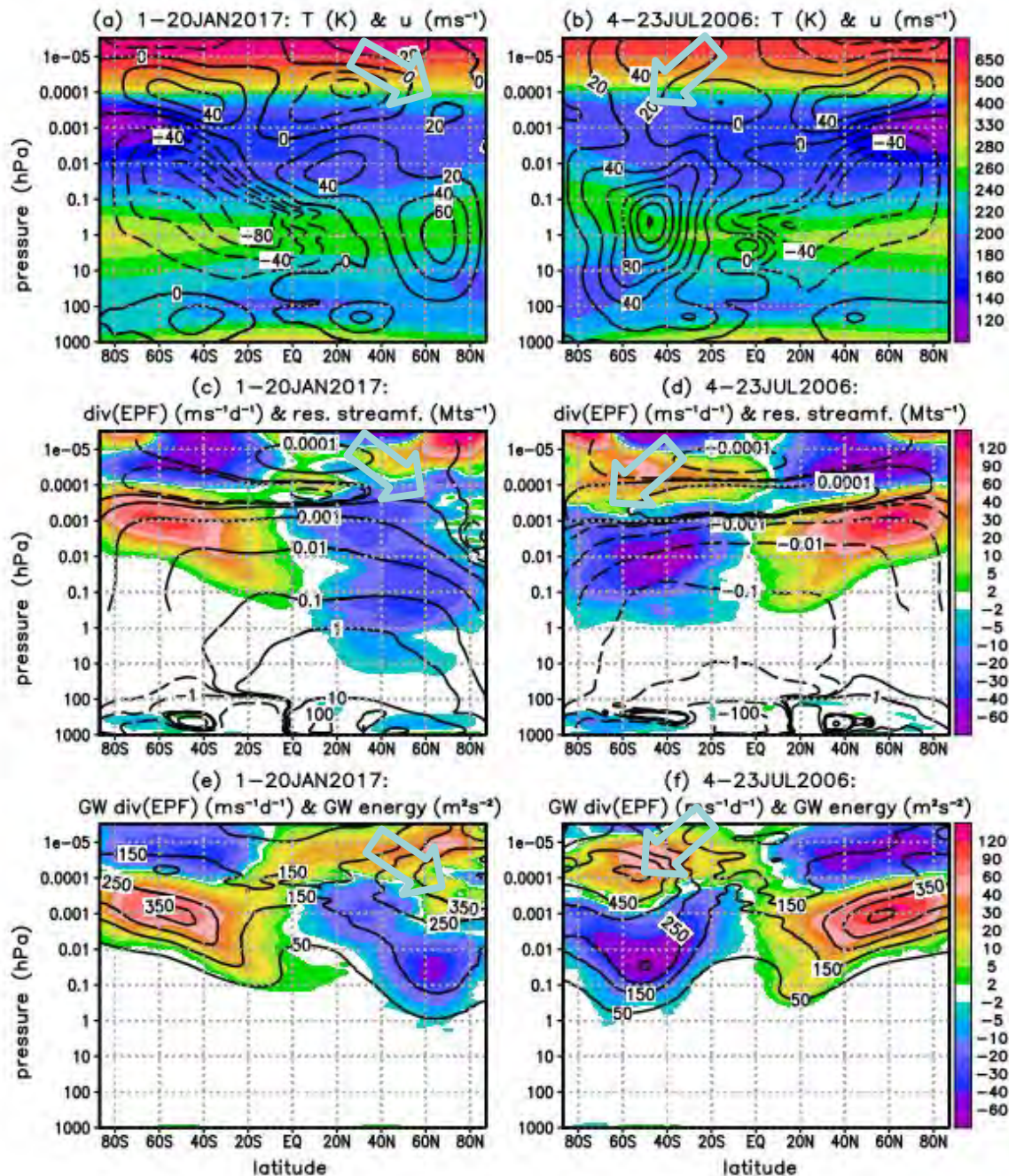
$$\Phi^{nh}|_{p_i} \approx -\int_{p_i}^{p_1} \left(\frac{RT}{pg} \right)^2 \left(\dot{p} D + \int_0^p \partial_t D d\hat{p} + \mathbf{v} \cdot \int_0^p \nabla D d\hat{p} \right) dp$$

$$\Phi^{nh}|_{p_1} = 0, \quad p_1 = 100 \text{ hPa}$$

Semi-implicit time stepping includes the actual global-mean temperature, the global-mean diffusion coefficients, and the non-hydrostatic correction.

The HIAMCM also employs the time filter of Williams (2009, MWR) to better suppress computational modes.

Implication for the generation circulation when GWs are resolved

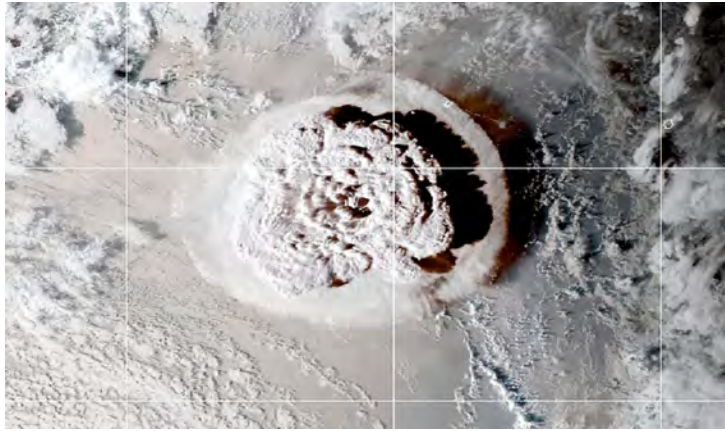


- Continuously eastward zonal wind in the winter mesopause region at high latitudes.
- Eastward drag and very large amplitudes from (presumably secondary) GWs ($\lambda_h < 1350$ km) in the winter mesopause region.
- **Effects are stronger in the SH than in the NH, that is for a stronger polar vortex.**
- Reversed residual circulation in the mesopause region extends from pole to pole during July, but not during January.

Model data from:
Becker & Oberheide, GRL, subm.

Sondary GWs caused by the Tonga eruption

Coupled model simulations using MESORAC-HIAMCM-SAMI3



The Tonga eruption caused massive perturbations in the lower atmosphere starting around 4:20 UT on 15 January 2022. These perturbations gave rise to high-frequency GWs that propagated to higher altitudes where they dissipated from breaking (MLT) and molecular viscosity (above ~110 km), giving rise to localized and intermittent body forces that generated secondary GWs.

- We infer **updrafts** from NOAA's Geostationary Operational Environmental Satellite (GOES) data, then use a convective plume/explosion model (Vadas, JGR, 2013) and ray tracing + reconstruction of the primary GW field (Vadas & Fritts, AG, 2009) to compute the **body forces from the dissipation of the primary, small-scale, and high-frequency GWs excited** by the Tonga eruption. This combination of tools is called the **Model for gravity wave SOURCE, Ray trAcing and reConstruction (MESORAC)** (Vadas et al., 2023, JGR-SP).
- We plug the **body forces** from MESORAC into **HIAMCM** to simulate the **secondary GWs**.
- The ionospheric model **SAMI3** (e.g., Huba et al., GRL, 2023) is then **driven by** the high-resolution **neutral dynamics from the HIAMCM** to study the **effects in the ionosphere**.